the presence of b- and y-series fragment ions of peptides of putative glycopeptides or molecular weight difference of sugar unit. The molecular weight of the carbohydrate in the glycopeptide was calculated from the molecular weights of the glycopeptide and the suggested peptide. The oligosaccharide composition and type were deduced from the molecular weight of the carbohydrate.

Oligosaccharide sequencing by exoglycosidase digestions

Trypsin in the digest of human CP was inactivated by boiling for 5 min at 100 °C. Aliquots of the digest (4 μg) were digested in a volume of 20 μl for 12 h at 37 °C in 50 mM sodium phosphate buffer (pH 5.0) using the following exoglycosidases alone or in combination: α2–3 neuraminidase, 20 mU/ml; α2–3,6,8,9 neuraminidase, 100 mU/ml; α1–3,4 fucosidase, 20 mU/ml; and β1–4 galactosidase, 30 mU/ml. Aliquots (0.08 μg) before and after exoglycosidase digestions were subjected to LC-ESI-MS at *m/z* 700 to 2000 in which MS/MS acquisition was not performed.

Results

Peptide mapping of tryptic digest of human CP (LC-ESI-MS/MS in m/z range of 400–2000)

The amino acid sequence of human CP (National Center for Biotechnology Information protein database: P00450) is shown in Fig. 1. The tryptic peptides, including potential N-glycosylation sites, are shown in bold type. Trypsin can digest human CP into seven glycopeptides containing only one potential N-glycosylation site. To determine the glycosylation state at each glycosylation site, we performed mass spectrometric peptide mapping of the tryptic digest of CP. An aliquot of 0.2 μg of the tryptic digest was analyzed by

KEKHYYIGII ETTWDYASDH GEKKLISVDT EHSNIYLQNG PDRIGRLYKK ALYLQYTDET
FRTTIEKPVW LGFLGPIIKA ETGDKVYVHL KNLASRPYTF HSHGITYYKE HEGAIYPDNT
TDFQRADDKV YPGEQYTYML LATEEQSPGE GDGNCVTRIY HSHIDAPKDI ASGLIGPLII
CKKDSLDKEK EKHIDREFVV MFSVVDENFS WYLEDNIKTY CSEPEKVDKD NEDFQESNRM
YSVNGYTFGS LPGLSMCAED RVKWYLFGMG NEVDVHAAFF HGQALTNKNY RIDTINLFPA
TLFDAYMVAQ NPGEWMLSCQ NLNHLKAGLQ AFFQVQECNK SSSKDNIRGK HVRHYYIAAE
EIIWNYAPSG IDIFTKENLT APGSDSAVFF EQGTTRIGGS YKKLVYREYT DASFTNRKER
GPEEEHLGIL GPVIWAEVGD TIRVTFHNKG AYPLSIEPIG VRFNKNNEGT YYSPNYNPQS
RSVPPSASHV APTETFTYEW TVPKEVGPTN ADPVCLAKMY YSAVDPTKDI FTGLIGPMKI
CKKGSLHANG RQKDVDKEFY LFPTVFDENE SLLLEDNIRM FTTAPDQVDK EDEDFQESNK
MHSMNGFMYG NQPGLTMCKG DSVVWYLFSA GNEADVHGIY FSGNTYLWRG ERRDTANLFP
QTSLTLHMWP DTEGTFNVEC LTTDHYTGGM KQKYTVNQCR RQSEDSTFYL GERTYYIAAV
EVEWDYSPQR EWEKELHHLQ EQNVSNAFLD KGEFYIGSKY KKVVYRQYTD STFRVPVERK
AEEEHLGILG PQLHADVGDK VKIIFKNMAT RPYSIHAHGV QTESSTVTPT LPGETLTYVW
KIPERSGAGT EDSACIPWAY YSTVDQVKDL YSGLIGPLIV CRRPYLKVFN PRRKLEFALL
FLVFDENESW YLDDNIKTYS DHPEKVNKDD EEFIESNKMH AINGRMFGNL QGLTMHVGDE
VNWYLMGMGN EIDLHTVHFH GHSFQYKHRG VYSSDVFDIF PGTYQTLEMF PRTPGIWLLH
CHVTDHIHAG METTYTVLQN EDTKSG

Fig. 1. Primary amino acid sequence of human CP (P00450). The tryptic peptides, including potential N-glycosylation sites, are shown in bold type. Tryptic peptides identified in the LC-ESI-MS/MS analysis are underlined. Cysteine residues are carboxymethylated. Identified N-glycosylation sites are indicated by arrow.

LC-ESI-MS/MS in the *m/z* range of 400–2000 (data not shown). When molecular ions with more than a single charge were detected, the product ion spectrum was acquired automatically. Peptide identification of each product ion spectrum was done using the Mascot search engine. More than 70% of the amino acid sequence was identified; identified amino acids of CP are underlined in Fig. 1. Three peptides containing the potential N-glycosylation site (Asn208, Asn569, and Asn907 [residues 197–218, 558–579, and 895–917, respectively]) were detected, whereas peptides containing the other N-glycosylation sites were not detected. Thus, Asn119, Asn339, Asn378, and Asn743 might be glycosylated.

Glycosylation analysis of human CP (LC-ESI-MS/MS in the m/z range of 1000–2000)

N-glycosylated peptides have relatively high molecular weights due to their oligosaccharide moiety. Because ions at lower *m/z* values can be detected in the *m/z* range of 400–2000, glycopeptide ions with higher *m/z* values might be missed to obtain product ion spectra. To detect glycopeptide ions preferentially, another LC-ESI-MS/MS analysis was carried out in the *m/z* range of 1000–2000 using an aliquot of 0.4 μg of the tryptic digest. Fig. 2A shows a total ion chromatogram (TIC) of a TOF-MS scan for the full scan *m/z* 1000–2000. Fig. 2B shows a TIC of the product ion scan. Because product ion spectra of glycopeptide precursor ions have abundant carbohydrate B-ions, *m/z* 204 (HexNAc), *m/z* 186 (HexNAc-H_2O), *m/z* 366 (HexHexNAc), and *m/z* 292 (NeuAc), the extracted ion chromatogram at *m/z* 204.05–204.15 (HexNAc, 204.08) of the product ion scan is illustrated in Fig. 2C. The extracted ion chromatogram at *m/z* 204.05–204.15 of product ion spectra provides a useful indication of the selection of glycopeptide precursor ions. The glycopeptide ions were assigned based on an examination of product ion spectra using the information on amino acid sequences of the peptides containing a putative N-glycosylation site.

Identification of Asn119 glycopeptide

The product ion spectrum of 1366.6 (+3) at 26 min, labeled by A in Fig. 2C, is shown in Fig. 3A. There were abundant oligosaccharide oxonium ions such as *m/z* 204 (HexNAc), *m/z* 366 (HexHexNAc), *m/z* 186 (HexNAc-H_2O), *m/z* 168 (HexNAc-$2H_2O$), *m/z* 274 (NeuAc-H_2O), and *m/z* 292 (NeuAc). Thus, this precursor ion was assigned as a glycopeptide. Several fragment ions consistent with b- and y-series fragment ions [24] derived from the peptide EHEGAIYPDN^{119}TTDFQR (residues 110–125) were detected together with several deamidated (−17) or dehydrogenated (−18) b- and y-series ions and y-series ions with the GlcNAc residue. Thus, the peptide moiety EHEGA IYPDNTTDFQR was suggested. The carbohydrate's molecular weight, 2223.0, was calculated by subtracting the theoretical molecular weight of the peptide (1891.8) from

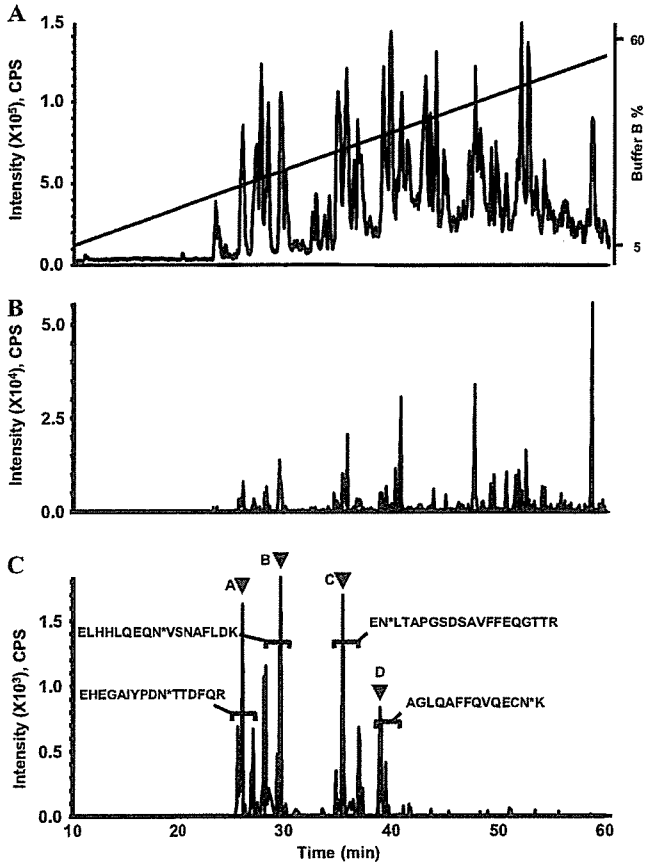

Fig. 2. LC-ESI-MS/MS in the *m/z* range of 1000–2000 of the tryptic digest of human CP. (A) TIC of the TOF-MS scan for the full-scan *m/z* 1000–2000 and the HPLC gradient. (B) TIC of the product ion scan acquired data-dependently. (C) Extracted ion chromatograph at *m/z* 204.05–204.15 of the product ion spectra. Brackets denote glycopeptide fraction and peptide sequences of the glycopeptides. Product ion spectra indicated by A–D are shown in Fig. 3.

the calculated molecular weight of the glycopeptide (4096.7) and adding the molecular weight of H_2O (18.0). The presence of product ions at *m/z* 274 (NeuAc-H_2O) and *m/z* 292 (NeuAc) suggested sialylation of the oligosaccharide. Thus, the carbohydrate's composition, $[HexNAc]_4[Hex]_5[NeuAc]_2$, was deduced.

Identification of Asn743 glycopeptide

The product ion spectrum of 1628.4 (+3) at 29 min, labeled by B in Fig. 2C, is shown in Fig. 3B. This precursor ion was assigned as a glycopeptide due to the presence of abundant oligosaccharide oxonium ions such as *m/z* 204 (HexNAc), *m/z* 366 (HexHexNAc), and *m/z* 292 (NeuAc) in the product ion spectrum. Several fragment ions were consistent with theoretical b- and y-series fragment ions derived from the peptide ELHHLQEQN^{743}VSNAFLDK (residues 735–751). Doubly charged ions of peptide (*m/z* 1011.7), peptide + HexNAc (*m/z* 1113.1), peptide + 2HexNAc (*m/z* 1214.6), peptide + 2HexNAc + Hex (*m/z* 1295.5), peptide + 2HexNAc + 2Hex (*m/z* 1376.7), and peptide + 2HexNAc + 3Hex (*m/z* 1457.5) showed the sequential fragmentation of the pentasaccharide carbohydrate core. The carbohydrate's molecular weight, 2879.1, was calculated from the theoretical molecular weight of the peptide (2021.0) and the calculated molecular weight of the glycopeptide (4882.1). The carbohydrate's composition, $[HexNAc]_5[Hex]_6[NeuAc]_3$, was deduced from the molecular weight.

Identification of Asn378 glycopeptide

The product ion spectrum of 1444.6 (+3) at 35 min, labeled by C in Fig. 2C, is shown in Fig. 3C. Abundant oligosaccharide oxonium ions were detected, as were several fragment ions consistent with b- and y-series fragment ions derived from the peptide EN^{378}LTAPGSDSAVFFEQGTTR (residues 377–391). The carbohydrate's molecular weight, 2222.9, was calculated from the theoretical molecular weight of the peptide (2126.0) and the calculated molecular weight of the glycopeptide (4330.9). Thus, the peptide moiety ENLTAPGSDSAVFFEQGTTR and the carbohydrate's composition, $[HexNAc]_4[Hex]_5[NeuAc]_2$, were suggested.

Identification of Asn339 glycopeptide

The product ion spectrum of 1282.6 (+3) at 39 min, labeled by D in Fig. 2C, is shown in Fig. 3C. The spectrum contains abundant oligosaccharide oxonium ions, and several fragment ions consistent with b- and y-series fragment ions derived from the peptide AGLQAFFQVQECN^{339}K (residues 327–340) were detected. The product ion spectrum contains the ions of the peptide (*m/z* 1640.8) and peptide + HexNAc (*m/z* 1843.9) and several y-series fragment ions of the peptide with a GlcNAc residue. The carbohydrate's molecular weight, 2223.0, was calculated from the theoretical molecular weight of the peptide (1639.7) and the calculated molecular weight of the glycopeptide (3844.7). Thus, the peptide moiety AGLQAFFQVQECNK and the carbohydrate's composition, $[HexNAc]_4[Hex]_5[NeuAc]_2$, were suggested.

Heterogeneity of oligosaccharides at each glycosylation site

Glycopeptides with the potential N-glycosylation sites Asn119, Asn339, Asn378, and Asn743 were detected, whereas no glycopeptides containing the other sites (Asn208, Asn569, and Asn907) could be detected in this LC-ESI-MS/MS analysis. These findings suggest that Asn119, Asn339, Asn378, and Asn743 of human CP are glycosylated and that Asn208, Asn569, and Asn907 are not. Once a glycopeptide was identified, the other glycopeptides with the same peptide could be easily assigned because they were eluted at a similar retention time in the order of the number of NeuAc and had similar product ion spectra and molecular weight difference of sugar units. The oligosaccharide heterogeneity at each four N-glycosylation sites was determined by mass spectrum. For a representative example, the mass spectrum of the glycopeptides containing

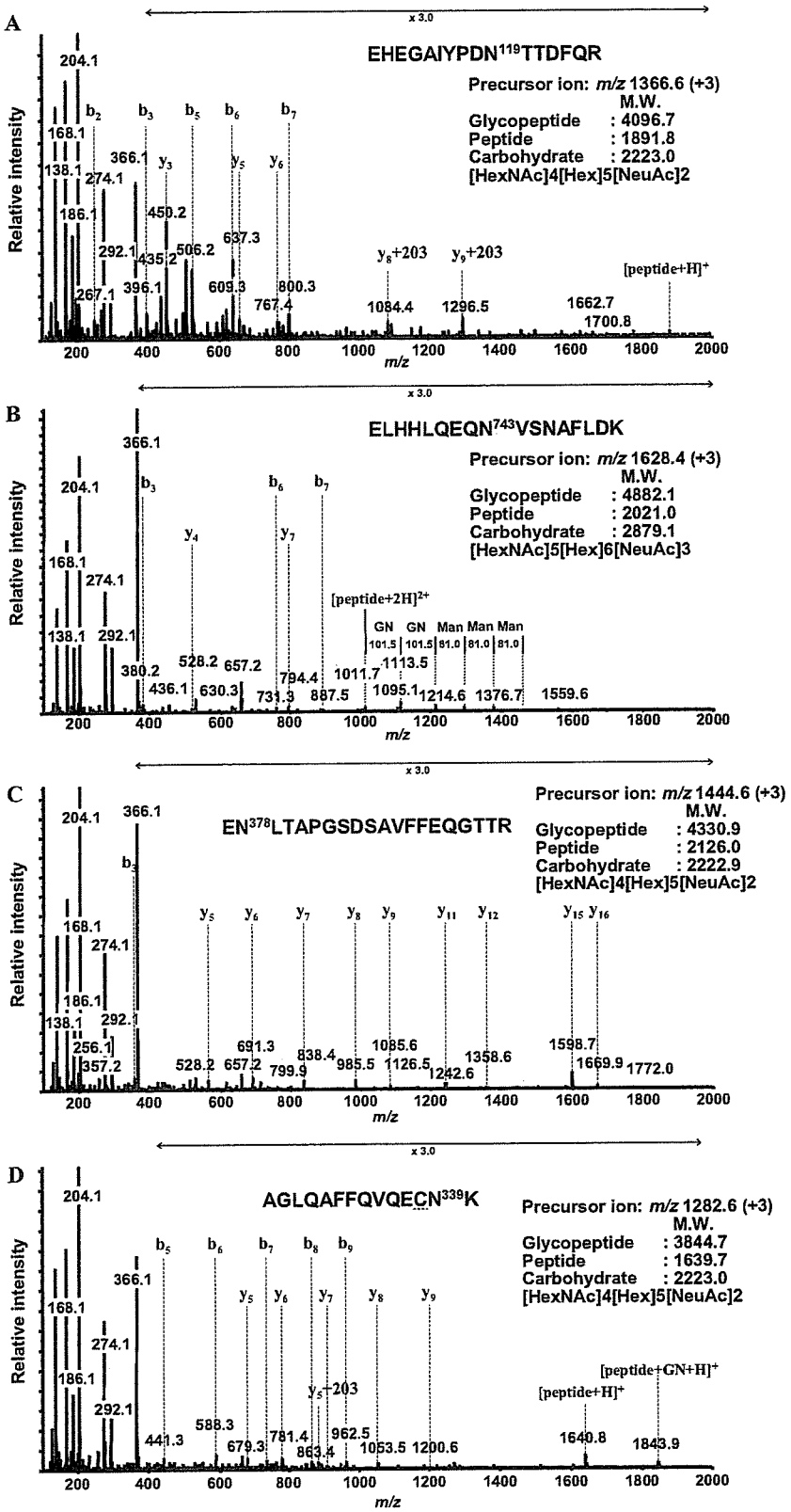

Fig. 3. Product ion spectra of *m/z* 1366.6 (+3) at 26 min (A), *m/z* 1628.4 (+3) at 29 min (B), *m/z* 1444.6 (+3) at 35 min (C), and *m/z* 1282.6 (+3) at 39 min (D) labeled by A, B, C, and D, respectively, in Fig. 2C. These spectra show abundant carbohydrate-derived ions at *m/z* 168 (HexNAc-$2H_2O$), *m/z* 186 (HexNAc-H_2O), *m/z* 204 (HexNAc), *m/z* 366 (HexHexNAc), *m/z* 274 (NeuAc-H_2O), and *m/z* 292 (NeuAc). The b- and y-series fragment ions [24] derived from the peptide moiety were observed. The molecular weights of the oligosaccharide were calculated from the molecular weights of the glycopeptide and peptide, and the deduced oligosaccharide composition is presented. Cystein residue was carboxymethylated.

Asn743 at 27.5 to 31.5 min is shown Fig. 4. The results of glycosylation analysis are summarized in Table 1. Deduced compositions of the oligosaccharides are estimated based on the calculated molecular weights of the oligosaccharides. Relative peak intensity was calculated by comparing triply charged glycopeptide ions. All glycosylation sites were occupied by at least three kinds of oligosaccharides, namely disialobiantennary structures ($[HexNAc]_4[Hex]_5[NeuAc]_2$), disialobiantennary structures with fucose ($[HexNAc]_4[Hex]_5[NeuAc]_2[Fuc]_1$), and trisialotriantennary structures ($[HexNAc]_5[Hex]_6[NeuAc]_3$). Trisialotriantennary structures with one fucose or two fucoses ($[HexNAc]_5[Hex]_6[NeuAc]_3[Fuc]_{1-2}$) were also detected at Asn119 and Asn743; furthermore, tetrasialotetraantennary structures with no fucose or one fucose ($[HexNAc]_6[Hex]_7[NeuAc]_4[Fuc]_{0-1}$) were detected at Asn743.

Linkage analysis of oligosaccharides by exoglycosydase digestion

To elucidate the oligosaccharide structure in terms of sequence and linkage, aliquots of the tryptic digest were further digested with exoglycosidases. As a representative example, Fig. 5 shows integrated mass spectra during the periods at which Asn119 glycopeptides were eluted in LC-ESI-MS analyses before and after digestion with exoglycosidase arrays. Treatment with α2–3 neuraminidase removed one NeuAc residue from most of the triantennary structures ($[HexNAc]_5[Hex]_6[NeuAc]_3[Fuc]_{0-2}$) and a small amount of biantennary structures ($[HexNAc]_4[Hex]_5[NeuAc]_2[Fuc]_{0-1}$) (Fig. 5B). A minor amount of triantennary structures removed two NeuAc residues. Thus, it appears that most triantennary structures contain one α2–3-linked NeuAc. Treatment with α2–3 neuraminidase + β1–4 galactosidase removed all terminal galactose residues from the desialylated glycans without fucose residues but only partially digested terminal galactoses from the desialylated glycans with fucoses (Fig. 5C). The addition of α1–3,4 fucosidase to α2–3 neuraminidase + β1–4 galactosidase treatment completely digested the remaining terminal galactose by releasing one fucose and one galactose (Fig. 5D). Thus, galactose residues are linked β1–4 to GlcNAc, and undigestion of terminal galactose by β1–4 galactosidase is due to attachment of fucose [25,26]. Because galactose was linked to GlcNAc in the β1–4 position, the fucose removed with α1–3,4 fucosidase may be linked α1–3 to GlcNAc but not α1–4 to GlcNAc. These data strongly suggested that sialyl Lewis X structure was present in human CP. Sialyl Lewis X structure was present predominantly in triantennary oligosaccharides, but a small amount seemed to be present in biantennary oligosaccharides as well. The remaining fucose residue may be linked α1–6 to reducing end GlcNAc (core fucose).

Fig. 6 shows integrated mass spectra of Asn119, Asn743, Asn378, and Asn339 glycopeptides in LC-ESI-MS analysis following digestion with α2–3,6,8,9 neuraminidase + β1–4 galactosidase. Treatment with α2–3,6,8,9 neuraminidase + β1–4 galactosidase removed all NeuAc and then removed terminal galactoses in the outer arms without fucose. Thus, this treatment could differentiate glycoforms based on the location of fucose residues. Fucosylation occurred predominantly at reducing end GlcNAc in biantennary oligosaccharides and occurred at reducing end GlcNAc and/or outer arm GlcNAc in triantennary oligosaccharides. Mass spectra of Asn119 and Asn743 glycopeptides showed higher oligosaccharide heterogeneity, and a minor amount of tetraantennary glycans could be detected. The glycosylation profile

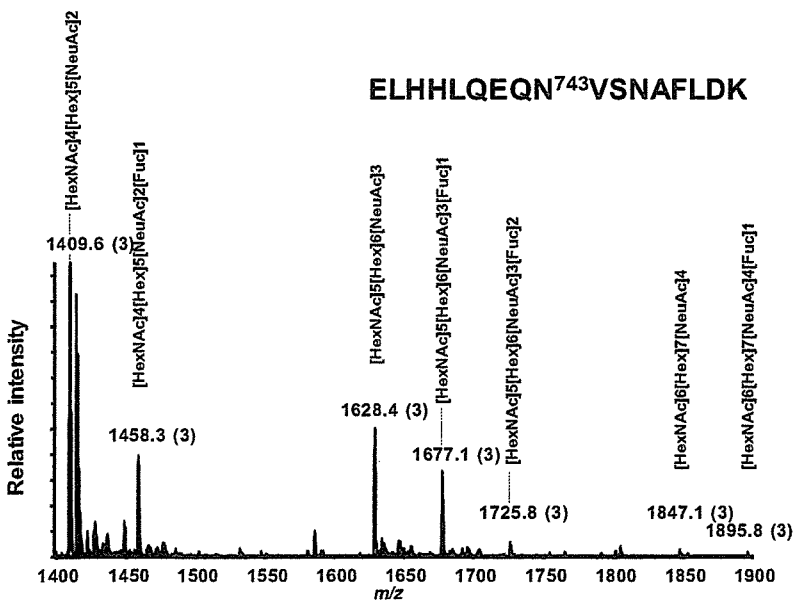

Fig. 4. Mass spectrum of the glycopeptides containing Asn743 eluting at 27.5–31.5 min from Fig. 2A. Deduced composition of the oligosaccharides is indicated based on the molecular weights of the oligosaccharides.

Table 1
Results of site-specific glycosylation analysis of human CP

Retention time (min)	Glycopeptides		Calculated MW	Relative peak intensity[a] (%)	Peptide		Oligosaccharide		
	m/z	Charge			Sequence	Theoretical MW	Calculated MW	Theoretical MW	Composition[b,c]
26	1415.3	+3	4242.8	52	EHEGAIYPDN[1119]TTDFQR	1891.8	2369.0	2368.8	[HexNAc]4[Hex]5[NeuAc]2[Fuc]1
26	1366.6	+3	4096.7	100	EHEGAIYPDN[1119]TTDFQR	1891.8	2223.0	2222.8	[HexNAc]4[Hex]5[NeuAc]2
27	1682.7	+3	5045.1	6	EHEGAIYPDN[1119]TTDFQR	1891.8	3171.3	3171.1	[HexNAc]5[Hex]6[NeuAc]3[Fuc]2
27	1634.0	+3	4899.0	21	EHEGAIYPDN[1119]TTDFQR	1891.8	3025.2	3025.1	[HexNAc]5[Hex]6[NeuAc]3[Fuc]1
27	1225.8	+4	4899.0						
27	1585.3	+3	4753.0	24	EHEGAIYPDN[1119]TTDFQR	1891.8	2879.2	2879.0	[HexNAc]5[Hex]6[NeuAc]3
27	1189.3	+4	4753.0						
28	1458.3	+3	4372.0	35	ELHHLQEQN[743]VSNAFLDK	2021.0	2369.0	2368.8	[HexNAc]4[Hex]5[NeuAc]2[Fuc]1
28	1409.6	+3	4225.9	100	ELHHLQEQN[743]VSNAFLDK	2021.0	2222.9	2222.8	[HexNAc]4[Hex]5[NeuAc]2
28	1057.5	+4	4225.9						
29	1725.8	+3	5174.5	5	ELHHLQEQN[743]VSNAFLDK	2021.0	3171.5	3171.1	[HexNAc]5[Hex]6[NeuAc]3[Fuc]2
29	1294.6	+4	5174.2						
29	1677.1	+3	5028.2	29	ELHHLQEQN[743]VSNAFLDK	2021.0	3025.3	3025.1	[HexNAc]5[Hex]6[NeuAc]3[Fuc]1
29	1258.1	+4	5028.2						
29	1628.4	+3	4882.1	43	ELHHLQEQN[743]VSNAFLDK	2021.0	2879.1	2879.0	[HexNAc]5[Hex]6[NeuAc]3
29	1221.5	+4	4882.1						
31[d]	1895.8	+3	5684.4	2	ELHHLQEQN[743]VSNAFLDK	2021.0	3681.4	3681.3	[HexNAc]6[Hex]7[NeuAc]4[Fuc]1
31[d]	1422.1	+4	5684.3						
31[d]	1847.1	+3	5538.4	3	ELHHLQEQN[743]VSNAFLDK	2021.0	3535.4	3535.2	[HexNAc]6[Hex]7[NeuAc]4
31	1385.6	+4	5538.3						
35[d]	1493.3	+3	4477.0	6	EN[378]LTAPGSDSAVFFEQGTTR	2126.0	2369.0	2368.8	[HexNAc]4[Hex]5[NeuAc]2[Fuc]1
35	1444.6	+3	4330.9	100	EN[378]LTAPGSDSAVFFEQGTTR	2126.0	2222.9	2222.8	[HexNAc]4[Hex]5[NeuAc]2
37	1712.1	+3	5133.2	8	EN[378]LTAPGSDSAVFFEQGTTR	2126.0	3025.2	3025.1	[HexNAc]5[Hex]6[NeuAc]3[Fuc]1
37	1284.3	+4	5133.2						
37	1663.4	+3	4987.1	23	EN[378]LTAPGSDSAVFFEQGTTR	2126.0	2879.2	2879.0	[HexNAc]5[Hex]6[NeuAc]3
37	1247.8	+4	4987.2						
39	1331.3	+3	3990.8	14	AGLQAFFQVQECN[339]K	1639.7	2369.1	2368.8	[HexNAc]4[Hex]5[NeuAc]2[Fuc]1
39	1923.4	+2	3844.7		AGLQAFFQVQECN[339]K	1639.7	2223.0	2222.8	[HexNAc]4[Hex]5[NeuAc]2
39	1282.6	+3	3844.7	100					
41	1501.3	+3	4500.8	6	AGLQAFFQVQECN[339]K	1639.7	2879.2	2879.0	[HexNAc]5[Hex]6[NeuAc]3

Note. All masses are monoisotopic. Cysteine residue was carboxymethylated.

[a] Relative peak intensity was calculated by comparing same charge state glycopeptide ions. The intensity of the glycoform with maximum at each glycosylation site was taken as 100%.

[b] The oligosaccharide composition was deduced from the molecular weight of the oligosaccharide.

[c] The glycopeptide ions adducted by NH_4^+ or Na^+ were excluded.

[d] Product ion spectra of these molecular ions were not acquired. However, these were considered glycopeptides because of a molecular weight difference of 146 (Fuc) and the same retention time as other glycopeptides.

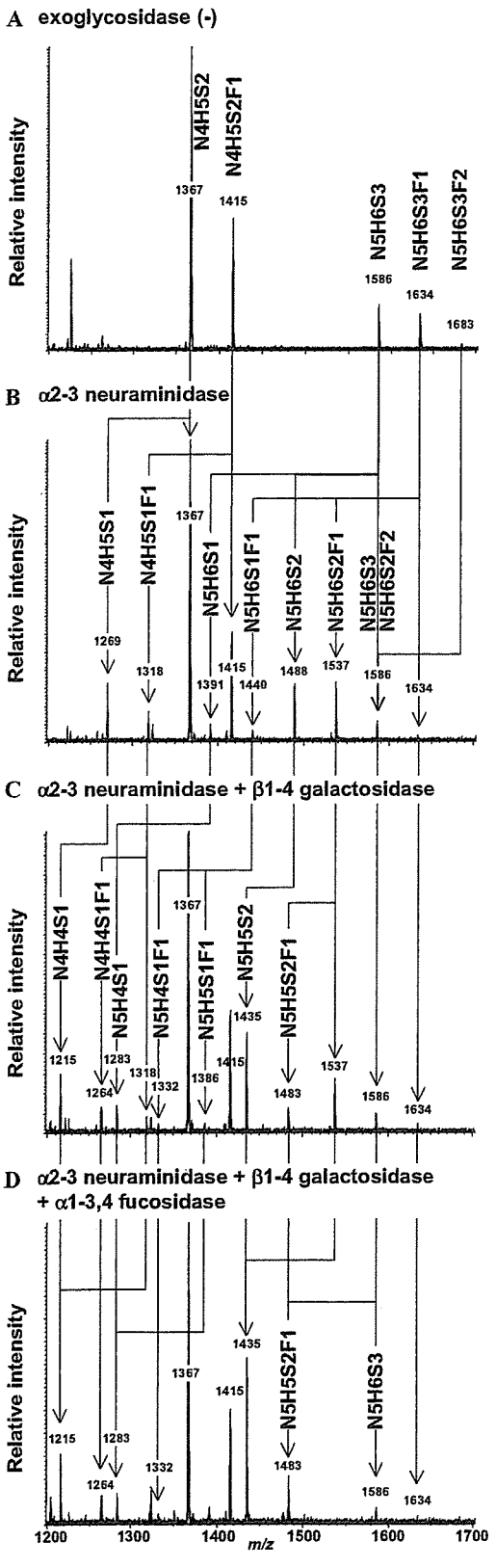

Fig. 5. LC-ESI mass spectra of the glycopeptides containing Asn119 digested with the following exoglycosidases: (A) exoglycosidase (–); (B) α2–3 neuraminidase; (C) α2–3 neuraminidase + β1–4 galactosidase; (D) α2–3 neuraminidase + β1–4 galactosidase + α1–3,4 fucosidase. Arrows between panels A and B, panels B and C, and panels C and D correspond to the digestion of NeuAc, Gal, and Gal+Fuc, respectively. H, hexose; N, *N*-acetylhexosamine; F, fucose; S, *N*-acetylneuraminic acid.

of Asn378 glycopeptides showed lower core fucosylation, and that of Asn339 glycopeptides showed lower branching. These glycosylation profiles provided the heterogeneity of fucose linkage and the number of arms at each glycosylationsite in human CP.

Discussion

A site-specific glycosylation analysis of human CP was conducted using LC-ESI-MS/MS, where product ion spectra were acquired in a data-dependent manner. The collision energy for the product ion scan was adjusted from 30 to 80 eV depending on the size and charge of the precursor ion. Under these conditions, peptide precursor ions were degraded and produced b- and y-series fragment ions derived from the amino acid sequence. Glycopeptide precursor ions produced abundant carbohydrate ions (*m/z* 204, 186, 168, and 366) together with several low intensity b- and y-series fragment ions derived from the amino acid sequence [20,21]. Thus, product ion spectra of glycopeptides are readily distinguishable from those of peptides by such carbohydrate marker ions, and the peptide moiety in the glycopeptide could be deduced from the product ions that were consistent with the expected fragment ions derived from the peptide containing the N-glycosylation site. It is known that the glycopeptide ions are more labile than peptide ions and produce consecutive monosaccharide/polysaccharide losses at much lower collision energy, and this would provide information about branching and fucose location [18]. However, we used relatively high collision energy in this site-specific glycosylation analysis to identify the peptide ions in parallel with the detection and identification of the glycopeptide ions.

Protein coverage of more than 70% in human CP was obtained in the LC-ESI-MS/MS analysis with the *m/z* range of 400–2000 (for peptide mapping). The heterogeneity at four potential N-glycosylation sites was determined in the *m/z* range of 1000–2000 (glycosylation analysis). We could detect all of the potential glycosylation sites as either glycopeptides or nonglycosylated peptides. Peptides containing the potential N-glycosylation site Asn208, Asn569, or Asn907 were detected in nonglycosylated but not glycosylated forms. Peptides with the potential N-glycosylation site Asn119, Asn339, Asn378 or Asn743 were detected in glycosylated but not nonglycosylated forms. These findings indicate that Asn119, Asn339, Asn378, and Asn743 of human CP are glycosylated and that Asn208, Asn569, and Asn907 are not. Human CP was reported to have no O-linked glycosylation [8]. No information on O-glycosylation was obtained from this analysis. These results are consistent with a previous study determining the glycosylation sites of human CP [9].

Heterogeneity of oligosaccharides was determined at each of four glycosylation sites. Disialobiantennary structures with no fucose or one fucose ($[HexNAc]_4$ $[Hex]_5$ $[NeuAc]_2[Fuc]_{0-1}$) and trisialotriantennary structures

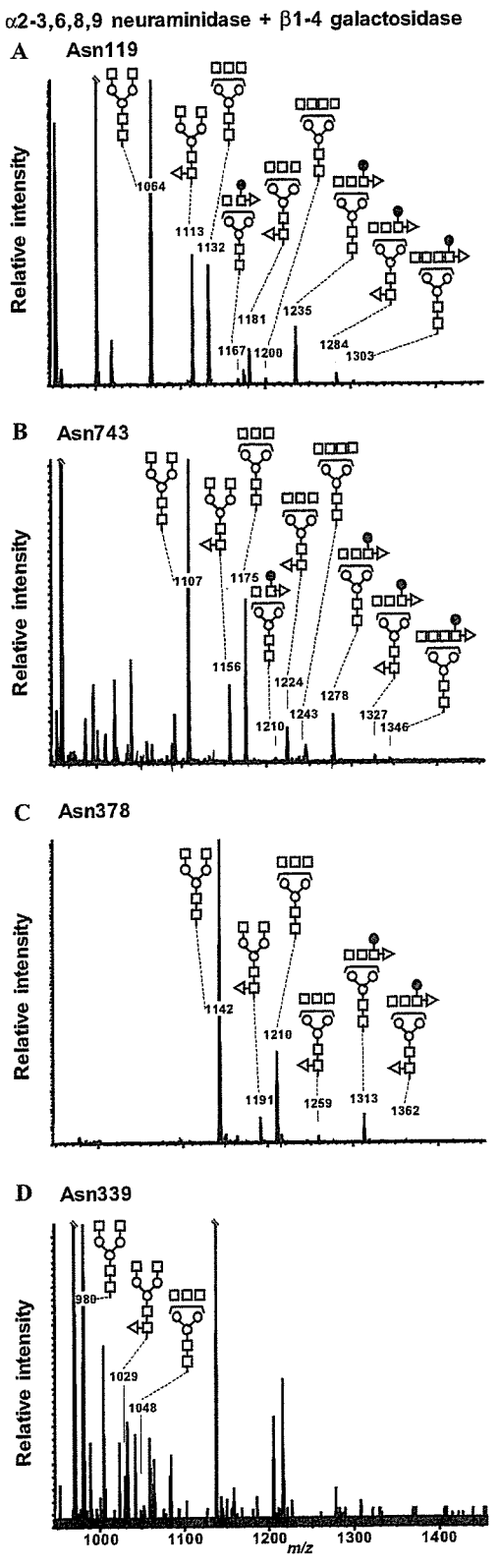

Fig. 6. LC-ESI mass spectra of the glycopeptides containing Asn119 (A), Asn743 (B), Asn378 (C), and Asn339 (D) after digestion with α2–3,6,8,9 neuraminidase + β1–4 galactosidase. Glycosylation profiles showed different degrees of branching and fucosylation at core GlcNAc and outer arm GlcNAc between glycosylation sites. Open circles, mannose; closed circles, galactose; open squares, *N*-acetyl glucosamine; open triangles, fucose.

($[HexNAc]_5[Hex]_6[NeuAc]_3$) were observed at all sites. These dominant oligosaccharides were consistent with structures published previously [7,8]. Furthermore, we detected trisialotriantennary structures with one fucose ($[HexNAc]_5[Hex]_6[NeuAc]_3[Fuc]_1$) at Asn119, Asn378, and Asn743, trisialotriantennary structures with two fucoses ($[HexNAc]_5[Hex]_6[NeuAc]_3[Fuc]_2$) at Asn119 and Asn743, and tetrasialotetraantennary structures with no fucose or one fucose ($[HexNAc]_6[Hex]_7[NeuAc]_4[Fuc]_{0-1}$) at Asn743.

To determine the linkage of fucose and NeuAc, exoglycosidase digestions were performed. Treatment with α2–3 neuraminidase suggested that roughly one antenna of triantennary glycans was linked by NeuAc in the α2–3 position. This is consistent with the previous findings that NeuAc is linked α2–3 to the Galβ1–4GlcNAcβ1–4Manα1–3Manβ1–4GlcNAcβ1–4GlcNAc group in the triantennary glycan in human CP [7,8]. Results from α2–3 neuraminidase + β1–4 galactosidase treatments with or without α1–3,4 fucosidase suggested that fucose residues were linked to reducing end GlcNAc and/or outer arm GlcNAc in the α1–3 position in the antenna where NeuAc is linked to galactose in the α2–3 position. These findings indicated that human CP contains a certain amount of sialyl Lewis X structure in triantennary glycans. Treatment with α2–3,6,8,9 neuraminidase + β1–4 galactosidase reveals the heterogeneity of the location of fucosylation as well as the number of arms. Although relative peak intensity does not express the relative amount of each glycan due to the different ionization efficiencies, the mass spectra showed the difference in fucosylation pattern and number of arms among sites.

No asialo oligosaccharides were detected in this analysis. It is known that desialylated CP is rapidly cleared from the circulation by the asialoglycoprotein receptor within the parenchymal cells of liver [27,28]. It is possible that desialylated CP might be cleared immediately by the liver.

Although the N-linked carbohydrate structures linked to human CP have been studied, only a few carbohydrate structures have been reported and site-specific characterization of these oligosaccharides has not been described. To determine the glycosylation state at each glycosylation site, the tryptic digest was examined by LC-ESI-MS/MS, where product ion spectra were acquired data-dependently. Glycopeptide ions were assigned based on the product ion spectra. Fucose and NeuAc linkages were determined by exoglycosidase digestions. Our data successfully provided comprehensive information on the site-specific N-linked oligosaccharides in human CP. This method is a powerful technique for elucidating the glycosylation of a biological sample.

Acknowledgments

This study was supported by a Grant-in-Aid for Research on Health Sciences focusing on Drug Innovation from the Japan Health Sciences Foundation.

References

[1] S. Osaki, D.A. Johnson, E. Frieden, The possible significance of the ferrous oxidase activity of ceruloplasmin in normal human serum, J. Biol. Chem. 241 (1966) 2746–2751.

[2] K. Yoshida, K. Furihata, S. Takeda, A. Nakamura, K. Yamamoto, H. Morita, S. Hiyamuta, S. Ikeda, N. Shimizu, N. Yanagisawa, A mutation in the ceruloplasmin gene is associated with systemic hemosiderosis in humans, Nat. Genet. 9 (1995) 267–272.

[3] Z.L. Harris, Y. Takahashi, H. Miyajima, M. Serizawa, R.T. MacGillivray, J.D. Gitlin, Aceruloplasminemia: molecular characterization of this disorder of iron metabolism, Proc. Natl. Acad. Sci. USA 92 (1995) 2539–2543.

[4] Z.L. Harris, A.P. Durley, T.K. Man, J.D. Gitlin, Targeted gene disruption reveals an essential role for ceruloplasmin in cellular iron efflux, Proc. Natl. Acad. Sci. USA 96 (1996) 10812–10817.

[5] N. Takahashi, T.L. Ortel, F.W. Putnam, Single-chain structure of human ceruloplasmin: the complete amino acid sequence of the whole molecule, Proc. Natl. Acad. Sci. USA 81 (1984) 390–394.

[6] M.L. Koschinsky, W.D. Funk, B.A. van Oost, R.T. MacGillivray, Complete cDNA sequence of human preceruloplasmin, Proc. Natl. Acad. Sci. USA 83 (1986) 5086–5090.

[7] K. Yamashita, C.J. Liang, S. Funakoshi, A. Kobata, Structural studies of asparagine-linked sugar chains of human ceruloplasmin. Structural characteristics of the triantennary complex type sugar chains of human plasma glycoproteins, J. Biol. Chem. 256 (1981) 1283–1289.

[8] M. Endo, K. Suzuki, K. Schmid, B. Fournet, Y. Karamanos, J. Montreuil, L. Dorland, H. van Halbeek, J.F. Vliegenthart, The structures and microheterogeneity of the carbohydrate chains of human plasma ceruloplasmin: a study employing 500-MHz ^{1}H-NMR spectroscopy, J. Biol. Chem. 257 (1982) 8755–8760.

[9] N. Takahashi, Y. Takahashi, T.L. Ortel, J.N. Lozier, N. Ishioka, F.W. Putnam, Purification of glycopeptides of human plasma proteins by high-performance liquid chromatography, J. Chromatogr. 317 (1984) 11–26.

[10] R.J. Cousins, Absorption, transport, and hepatic metabolism of copper and zinc: special reference to metallothionein and ceruloplasmin, Physiol. Rev. 65 (1985) 238–309.

[11] A. Mackiewicz, M.K. Ganapathi, D. Schultz, I. Kushner, Monokines regulate glycosylation of acute-phase proteins, J. Exp. Med. 166 (1987) 253–258.

[12] J.E. Hansen, J. Iversen, A. Lihme, T.C. Bog-Hansen, Acute phase reaction, heterogeneity, and microheterogeneity of serum proteins as nonspecific tumor markers in lung cancer, Cancer 60 (1987) 1630–1635.

[13] A. Senra Varela, J.J. Lopez Saez, D. Quintela Senra, Serum ceruloplasmin as a diagnostic marker of cancer, Cancer Lett. 121 (1997) 139–145.

[14] V. Ling, A.W. Guzzetta, E. Canova-Davis, J.T. Stults, W.S. Hancock, T.R. Covey, B.I. Shushan, Characterization of the tryptic map of recombinant DNA derived tissue plasminogen activator by high-performance liquid chromatography-electrospray ionization mass spectrometry, Anal. Chem. 63 (1991) 2909–2915.

[15] S.A. Carr, M.J. Huddleston, M.F. Bean, Selective identification and differentiation of N- and O-linked oligosaccharides in glycoproteins by liquid chromatography–mass spectrometry, Protein Sci. 2 (1993) 183–196.

[16] M.J. Huddleston, M.F. Bean, S.A. Carr, Collisional fragmentation of glycopeptides by electrospray ionization LC/MS and LC/MS/MS: methods for selective detection of glycopeptides in protein digests, Anal. Chem. 65 (1993) 877–884.

[17] P.A. Schindler, C.A. Settineri, X. Collet, C.J. Fielding, A.L. Burlingame, Site-specific detection and structural characterization of the glycosylation of human plasma proteins lecithin:cholesterol acyltransferase and apolipoprotein D using HPLC/electrospray mass spectrometry and sequential glycosidase digestion, Protein Sci. 4 (1995) 791–803.

[18] M.A. Ritchie, A.C. Gill, M.J. Deery, K. Lilley, Precursor ion scanning for detection and structural characterization of heterogeneous glycopeptide mixtures, J. Am. Soc. Mass Spectrom. 13 (2002) 1065–1077.

[19] F. Wang, A. Nakouzi, R.H. Angeletti, A. Casadevall, Site-specific characterization of the N-linked oligosaccharides of a murine immunoglobulin M by high-performance liquid chromatography/electrospray mass spectrometry, Anal. Biochem. 314 (2003) 266–280.

[20] J.F. Nemeth, G.P. Hochgesang Jr., L.J. Marnett, R.M. Caprioli, Characterization of the glycosylation sites in cyclooxygenase-2 using mass spectrometry, Biochemistry 40 (2001) 3109–3116.

[21] O. Krokhin, W. Ens, K.G. Standing, J. Wilkins, H. Perreault, Site-specific N-glycosylation analysis: matrix-assisted laser desorption/ionization quadrupole–quadrupole time-of-flight tandem mass spectral signatures for recognition and identification of glycopeptides, Rapid Commun. Mass Spectrom. 18 (2004) 2020–2030.

[22] A. Harazono, N. Kawasaki, T. Kawanishi, T. Hayakawa, Site-specific glycosylation analysis of human apolipoprotein B100 using LC/ESI MS/MS, Glycobiology 15 (2005) 447–462.

[23] C.W. Sutton, J.A. O'Neill, J.S. Cottrell, Site-specific characterization of glycoprotein carbohydrates by exoglycosidase digestion and laser desorption mass spectrometry, Anal. Biochem. 218 (1994) 34–46.

[24] P. Roepstorff, J. Fohlman, Proposal for a common nomenclature for sequence ions in mass spectra of peptides, Biomed. Mass Spectrom. 11 (1984) 601.

[25] K. Maemura, M. Fukuda, Poly-*N*-acetyllactosaminyl *O*-glycans attached to leukosialin: the presence of sialyl Le(x) structures in *O*-glycans, J. Biol. Chem. 267 (1992) 24379–24386.

[26] S. Hemmerich, S.D. Rosen, 6'-Sulfated sialyl Lewis X is a major capping group of GlyCAM-1, Biochemistry 33 (1994) 4830–4835.

[27] C.J. Van Den Hamer, A.G. Morell, I.H. Scheinberg, J. Hickman, G. Ashwell, Physical and chemical studies on ceruloplasmin: IX. The role of galactosyl residues in the clearance of ceruloplasmin from the circulation, J. Biol. Chem. 245 (1970) 4397–4402.

[28] A.G. Morell, G. Gregoriadis, I.H. Scheinberg, J. Hickman, G. Ashwell, The role of sialic acid in determining the survival of glycoproteins in the circulation, J. Biol. Chem. 246 (1971) 1461–1467.

The EMBO Journal (2006) 25, 5305–5316 | © 2006 European Molecular Biology Organization | All Rights Reserved 0261-4189/06
www.embojournal.org

THE EMBO JOURNAL

TRPC3 and TRPC6 are essential for angiotensin II-induced cardiac hypertrophy

Naoya Onohara[1], Motohiro Nishida[1], Ryuji Inoue[2], Hiroyuki Kobayashi[1], Hideki Sumimoto[3], Yoji Sato[4], Yasuo Mori[5], Taku Nagao[4] and Hitoshi Kurose[1,*]

[1]Department of Pharmacology and Toxicology, Graduate School of Pharmaceutical Sciences, Kyushu University, Higashi-ku, Fukuoka, [2]Department of Physiology, School of Medicine, Fukuoka University, Jonan-ku, Fukuoka, Japan, [3]Medical Institute of Bioregulation, Kyushu University, Higashi-ku, Fukuoka, Japan, [4]National Institute of Health Sciences, Setagaya, Tokyo, Japan and [5]Laboratory of Molecular Biology, Department of Synthetic Chemistry and Biological Chemistry, Graduate School of Engineering, Kyoto University, Kyoto, Japan

Angiotensin (Ang) II participates in the pathogenesis of heart failure through induction of cardiac hypertrophy. Ang II-induced hypertrophic growth of cardiomyocytes is mediated by nuclear factor of activated T cells (NFAT), a Ca^{2+}-responsive transcriptional factor. It is believed that phospholipase C (PLC)-mediated production of inositol-1,4,5-trisphosphate (IP_3) is responsible for Ca^{2+} increase that is necessary for NFAT activation. However, we demonstrate that PLC-mediated production of diacylglycerol (DAG) but not IP_3 is essential for Ang II-induced NFAT activation in rat cardiac myocytes. NFAT activation and hypertrophic responses by Ang II stimulation required the enhanced frequency of Ca^{2+} oscillation triggered by membrane depolarization through activation of DAG-sensitive TRPC channels, which leads to activation of L-type Ca^{2+} channel. Patch clamp recordings from single myocytes revealed that Ang II activated DAG-sensitive TRPC-like currents. Among DAG-activating TRPC channels (TRPC3, TRPC6, and TRPC7), the activities of TRPC3 and TRPC6 channels correlated with Ang II-induced NFAT activation and hypertrophic responses. These data suggest that DAG-induced Ca^{2+} signaling pathway through TRPC3 and TRPC6 is essential for Ang II-induced NFAT activation and cardiac hypertrophy.

The EMBO Journal (2006) **25**, 5305–5316. doi:10.1038/sj.emboj.7601417; Published online 2 November 2006
Subject Categories: signal transduction; molecular biology of disease
Keywords: angiotensin; cardiac hypertrophy; diacylglycerol; L-type Ca^{2+} channel; TRPC

Introduction

Regulators of cardiac function such as vasoactive neurotransmitters and hormones activate phospholipase C (PLC) and thereby generate inositol-1,4,5-trisphosphate (IP_3) and diacylglycerol (DAG). These agonists elevate the concentration of cytoplasmic free Ca^{2+} ($[Ca^{2+}]_i$) in cardiomyocytes, which induces positive inotropic effects on the heart and activates several transcriptional pathways that lead to cardiac hypertrophy (Wilkins and Molkentin, 2004; Woodcock and Matkovich, 2005). NFAT is one of the transcriptional factors regulated by $[Ca^{2+}]_i$ (Crabtree and Olson, 2002). The relevance of the NFAT signaling pathway to cardiac hypertrophy is underscored by the observation that cardiac-targeted transgenic animals expressing constitutively activated forms of either calcineurin or NFAT produced ventricular hypertrophy (Molkentin *et al*, 1998; Taigen *et al*, 2000). The Ca^{2+}-sensitive serine/threonine phosphatase (calcineurin) primarily regulates NFAT activity by rapid dephosphorylation of NFAT proteins and their translocation to the nucleus. A drop in nuclear Ca^{2+} deactivates calcineurin and allows one of several NFAT kinases to rephosphorylate NFAT, causing it to leave the nucleus and thereby inactivating transcription (Timmerman *et al*, 1996; Dolmetsch *et al*, 1997). Therefore, a sustained elevation of $[Ca^{2+}]_i$ is required for NFAT-dependent transcription.

The importance of agonists that activate PLC for cardiac hypertrophy is well established (Molkentin and Dorn, 2001). Many lines of evidence have shown that stimulation of PLC-linked G protein-coupled receptors, such as α_1-adrenergic receptor (Maruyama *et al*, 2002), Ang II receptor (Nishida *et al*, 2005) and endothelin receptor (Arai *et al*, 2003), induce hypertrophic growth of rat cardiac myocytes. More clinically relevant, hypertrophied hearts induced by volume overload are commonly characterized by high levels of IP_3-generating agonists such as Ang II (Dostal *et al*, 1992; Sadoshima *et al*, 1993). Numerous studies have demonstrated the need for sustained or periodic increases in $[Ca^{2+}]_i$ to cause the nuclear localization of NFAT (Dolmetsch *et al*, 1997; Tomida *et al*, 2003). In nonexcitable cells, IP_3 is generally accepted to function as a mediator of sustained Ca^{2+} responses (Timmerman *et al*, 1996; Dolmetsch *et al*, 1997). The sustained Ca^{2+} signaling requires the store-operated Ca^{2+} channel (SOC), which opens in response to depletion of intracellular stores through IP_3 receptor (IP_3R). Therefore, it is currently believed that Ca^{2+} entry through SOC regulates NFAT translocation. In the heart, however, the expression level of IP_3R is much lower than that of ryanodine receptor (Moschella and Marks, 1993). Voltage-dependent L-type Ca^{2+} channel and ryanodine receptor function as the major source of Ca^{2+} for normal Ca^{2+}-induced Ca^{2+} release of excitation–contraction (E–C) coupling, but many reports do not support the idea that the increase in $[Ca^{2+}]_i$ through E–C coupling between L-type Ca^{2+} channel and ryanodine receptor is coupled to NFAT activation (Wilkins and Molkentin, 2004).

A possible source of Ca^{2+} for activation of calcineurin is Ca^{2+} influx through transient receptor potential (TRP) proteins that are involved in store-operated Ca^{2+} entry (Clapham, 2003). Upregulation of canonical transient receptor potential (TRPC) proteins is recently reported to contribute to

*Corresponding author. Department of Pharmacology and Toxicology, Graduate School of Pharmaceutical Sciences, Kyushu University, 3-1-1 Maidashi, Higashi-ku, Fukuoka 812-8582, Japan.
Tel./Fax: +81 92 642 6884; E-mail: kurose@phar.kyushu-u.ac.jp

Received: 10 February 2006; accepted: 11 October 2006; published online: 2 November 2006

the development of cardiac hypertrophy (Seth *et al*, 2004). Other groups reported that TRPM7 regulates Mg^{2+} homeostasis, and TRPM6 and TRPM7 are differentially regulated by Ang II in vascular smooth muscle cells (He *et al*, 2005; Touyz *et al*, 2006). However, it is still unknown whether TRP channels contribute to receptor-stimulated activation of calcineurin-NFAT pathway in the heart. In this study, we investigated the mechanism of how Ang II stimulation induces the sustained Ca^{2+} signaling leading to NFAT activation and hypertrophic growth of rat neonatal cardiomyocytes.

Results

Essential role of DAG in Ang II-induced NFAT activation and cardiac hypertrophy

We first examined whether IP_3 or DAG is involved in Ang II-induced NFAT activation in rat neonatal cardiomyocytes. As it has been reported that pressure overload- and Ang II-induced cardiac hypertrophy are attenuated in NFAT4 (NFATc3)-null mice (Wilkins *et al*, 2002), the translocation of NFAT4 was determined in this study. Stimulation of cardiac myocytes with Ang II for 30 min increased the maximal nuclear predominant fluorescence of GFP-fused amino-terminal region of NFAT4 protein (GFP-NFAT4) (Figure 1A–C). The Ang II-induced NFAT translocation was completely suppressed by the expression of DAG kinase β (DGKβ), an enzyme that decreases the cellular DAG level by converting DAG to phosphatidic acid. Treatment with RHC80267, a DAG lipase inhibitor, significantly increased the Ang II-induced nuclear translocation of GFP-NFAT4. However, treatment with xestospongin C, an IP_3R blocker, did not affect the Ang II-induced translocation of GFP-NFAT4 to the nucleus. To directly inhibit IP_3-mediated signaling, we expressed the ligand-binding region of type 1 IP_3R (IP_3-sponge) (Uchiyama *et al*, 2002).

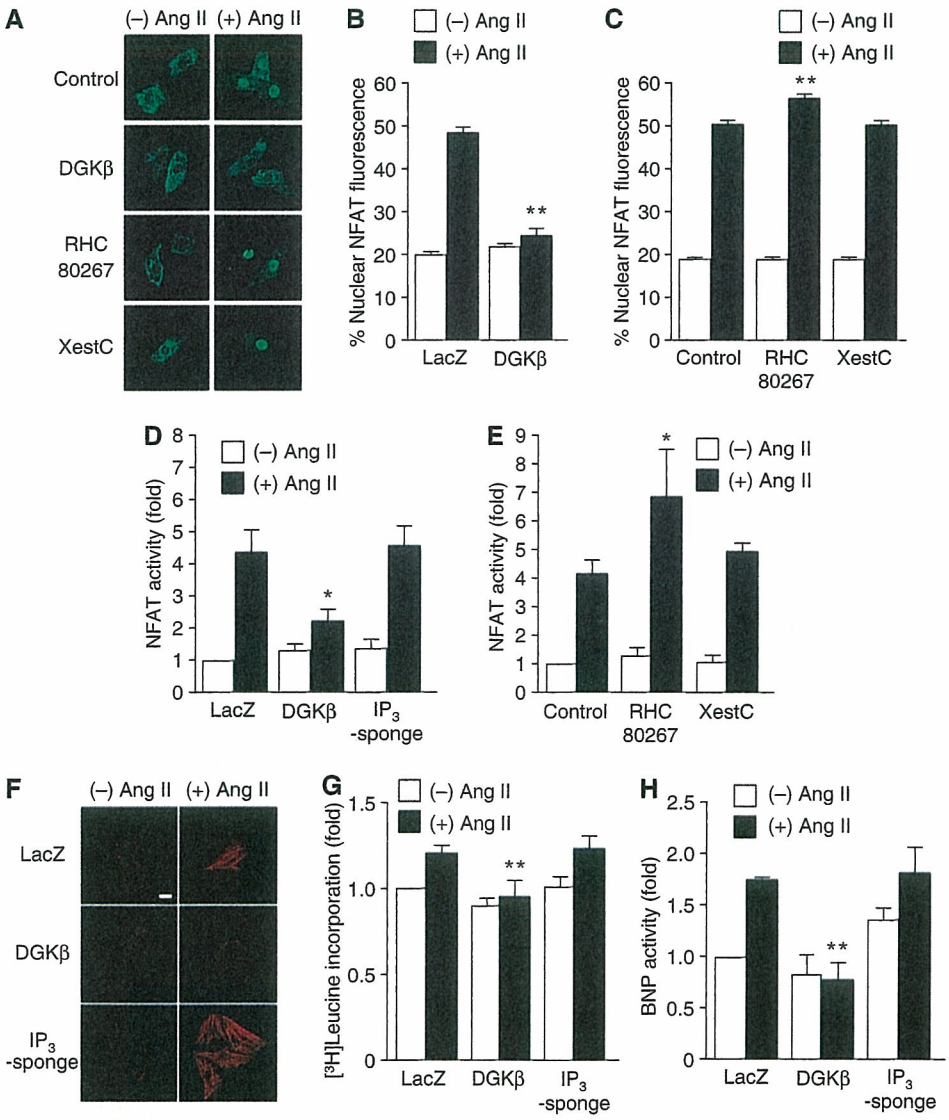

Figure 1 Essential role of DAG in Ang II-induced cardiomyocyte hypertrophy. (**A**) Nuclear translocation of GFP-NFAT4 by Ang II stimulation. A portion of cells was treated with RHC80267 (30 μM) or xestospongin C (XestC, 20 μM) for 30 min before the addition of Ang II (100 nM), and a portion of cells was infected with DGKβ for 48 h before Ang II stimulation. (**B**, **C**) Quantification of nuclear predominant fluorescence of GFP-NFAT4 after Ang II stimulation. (**D**, **E**) Effects of DGKβ, RHC80267, and XestC on the increase in NFAT-dependent luciferase activity by Ang II stimulation for 6 h. The fold activation was calculated by the values of untreated cells set as 1. (**F**–**H**) Effects of DGKβ and GFP-IP_3-sponge on Ang II-induced actin reorganization (**F**), protein synthesis (**G**), and BNP expression (**H**). Scale bar = 20 μm. $^*P<0.05$, $^{**}P<0.01$ versus control or LacZ-expressing cells.

The Ang II-induced transient increase in $[Ca^{2+}]_i$ (or Ca^{2+} release) was completely suppressed by the treatment with xestospongin C and by the expression of IP_3-sponge but not DGKβ (Supplementary Figure S1), suggesting the efficient inhibition of IP_3-mediated Ca^{2+} signaling. The Ang II-induced increase in NFAT-dependent luciferase reporter activity was suppressed by DGKβ, but not by xestospongin C and IP_3-sponge (Figure 1D and E). Treatment with RHC80267 promoted the Ang II-induced NFAT activation (Figure 1E). These results suggest the involvement of DAG in Ang II-induced NFAT activation. We also examined the involvement of DAG in Ang II-induced hypertrophic responses. Expression of DGKβ, but not IP_3-sponge, completely suppressed Ang II-induced hypertrophic responses, such as actin reorganization (Figure 1F), protein synthesis (Figure 1G), and expression of brain natriuretic peptide (BNP) (Figure 1H). These results suggest that DAG, but not IP_3, is essential for Ang II-induced NFAT activation and hypertrophic responses of neonatal cardiomyocytes.

Involvement of Ang II type 1 receptor, $G\alpha_q$, and PLC in Ang II-induced NFAT activation

In contrast to the absence of extracellular Ca^{2+} (Supplementary Figure S1A), myocytes showed spontaneous increases in $[Ca^{2+}]_i$ in the presence of extracellular Ca^{2+}. Treatment with Ang II induced the transient increase in $[Ca^{2+}]_i$ followed by sustained oscillatory increase in $[Ca^{2+}]_i$ (Figure 2A; the former can more clearly be seen in Supplementary Figure S1A). The Ca^{2+} oscillation represents a spontaneous activity of myocytes, and Ang II stimulation increased its frequency (Supplementary Figure S1C). The Ang II-induced Ca^{2+} response and NFAT activation were greatly suppressed by U73122, a PLC inhibitor, but not by U73343, an inactive analog of U73122 (Figure 2A–C). Thus, PLC primarily regulates Ang II-induced Ca^{2+} signal generation. The Ang II-induced translocation of GFP-NFAT4 was suppressed by CV11974, an Ang II type 1 receptor (AT1R) blocker, but not by PD123319, an AT2R blocker (Figure 2D). These results indicate that AT1R-mediated PLC activation is

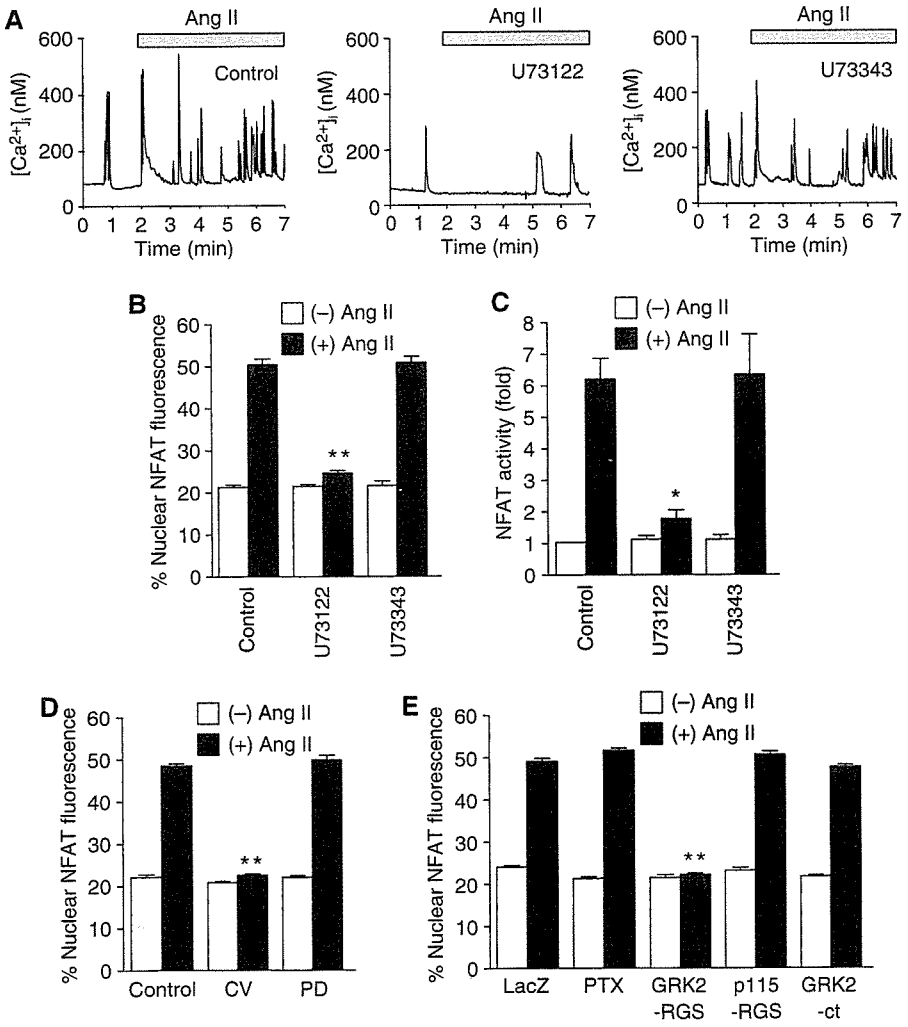

Figure 2 Involvement of AT1R, $G\alpha_q$, and PLC in Ang II-induced NFAT activation. (**A–C**) Effects of U73122 and U73343 on Ang II-induced Ca^{2+} responses (**A**), translocation of GFP-NFAT4 (**B**), and NFAT activation (**C**). (A) Effects of U73122 and U73343 on the increases in the frequency of Ca^{2+} oscillation during 5 min Ang II stimulation. The digital images were obtained every 1 s. (**D**) Effects of CV11974 and PD123319 on Ang II-induced NFAT translocation. Cells were treated with U73122 (5 μM), U73343 (5 μM), CV11974 (CV, 5 μM), or PD123319 (PD, 5 μM) for 30 min before the addition of Ang II (100 nM). (**E**) Effects of PTX, GRK2-RGS, p115-RGS, and GRK2-ct on Ang II-induced NFAT translocation. Cells were infected with adenovirus encoding LacZ (100 MOI), p115-RGS or GRK2-ct (100 MOI), or GRK2-RGS (300 MOI) for 48 h. A portion of cells was treated with PTX (100 ng/ml) for 24 h before Ang II stimulation. $^*P<0.05$, $^{**}P<0.01$ versus Ang II stimulation of control or LacZ-expressing cells.

involved in Ang II-induced NFAT4 activation. We next examined which G proteins are involved in Ang II-induced NFAT activation. It has been generally believed that $G\alpha_q$ plays an important role in agonist-induced cardiac hypertrophy (Molkentin and Dorn, 2001). To examine the involvement of $G\alpha_q$, we expressed regulator of G protein signaling (RGS) domain that is ~200 amino acids, specifically binds GTP-bound form of Gα and accelerates GTPase activity. When RGS domain is expressed in cells, it competes with activated form of Gα for endogenous effectors and accelerates turn-off reaction of Gα. Therefore, RGS domain can work as a specific inhibitor of Gα. As expected, the expression of a $G\alpha_q$-specific RGS domain of G protein-coupled receptor kinase 2 (GRK2-RGS) completely suppressed the Ang II-induced translocation of GFP-NFAT4 (Figure 2E). However, the expression of a $G\alpha_{12/13}$-specific RGS domain of p115RhoGEF (p115-RGS) did not affect the Ang II-induced translocation of GFP-NFAT4. *Pertussis* toxin (PTX) and carboxyl terminal region of GRK2 (GRK2-ct), a βγ subunit of G protein (Gβγ)-sequestering polypeptide, did not inhibit the Ang II-induced translocation of GFP-NFAT4 (Figure 2E). Thus, these results support the evidence that agonist-induced Ca^{2+}-dependent NFAT activation is predominantly regulated by $G\alpha_q$, but not by $G\alpha_{12/13}$, G_i or Gβγ in cardiomyocytes.

Requirement of Ca^{2+} influx through L-type Ca^{2+} channels and nonselective cation channels in Ang II-induced NFAT activation

It has been reported that DAG induces Ca^{2+} influx through activation of cation channels (Hofmann *et al*, 1999; Clapham, 2003). As the Ang II-induced periodic increase in $[Ca^{2+}]_i$ likely results from enhanced spontaneous activity of myocytes (which are dependent on extracellular Ca^{2+}; see above), and these were suppressed by DGKβ (Supplementary Figure S1), we next examined whether Ca^{2+} influx is involved in DAG-mediated responses. Treatment of cardiac myocytes with Ang II or with a DAG derivative, 1-oleoyl-2-acyl-*sn*-glycerol (OAG), increased the nuclear translocation of GFP-NFAT4 and NFAT activity, both of which were almost completely suppressed by the voltage-dependent Ca^{2+} channel blocker nitrendipine and a receptor-activated cation channel (RACC) inhibitor SK&F96365 (Figure 3A–C). As OAG-induced NFAT activation was also completely suppressed by cyclosporine A, a calcineurin inhibitor (Figure 3C), DAG increases NFAT activity through calcineurin activation. These results suggest that RACC and Ca^{2+} influx through L-type Ca^{2+} channel mediate Ang II- or DAG-induced NFAT activation.

Ang II activates DAG-sensitive cation channels in cardiac myocytes

To directly demonstrate that Ang II activates DAG-sensitive RACC, whole-cell patch-clamp experiments were performed. In quasi-physiological ionic conditions, administration of Ang II into the bath activated inward currents at −80 mV, which were further enhanced by RHC80267 (Figure 4A and B). These currents were completely abolished by *N*-methyl-D-glucamine substitution for all external cations (data not shown), and showed an outward-rectifying property with the reversal potential of ca. 0 mV (1.0±1.0 mV, $n=6$), when Cs^+ was intracellularly dialyzed via patch pipette and TTX (3 μM) and nitrendipine (1 μM) were added into

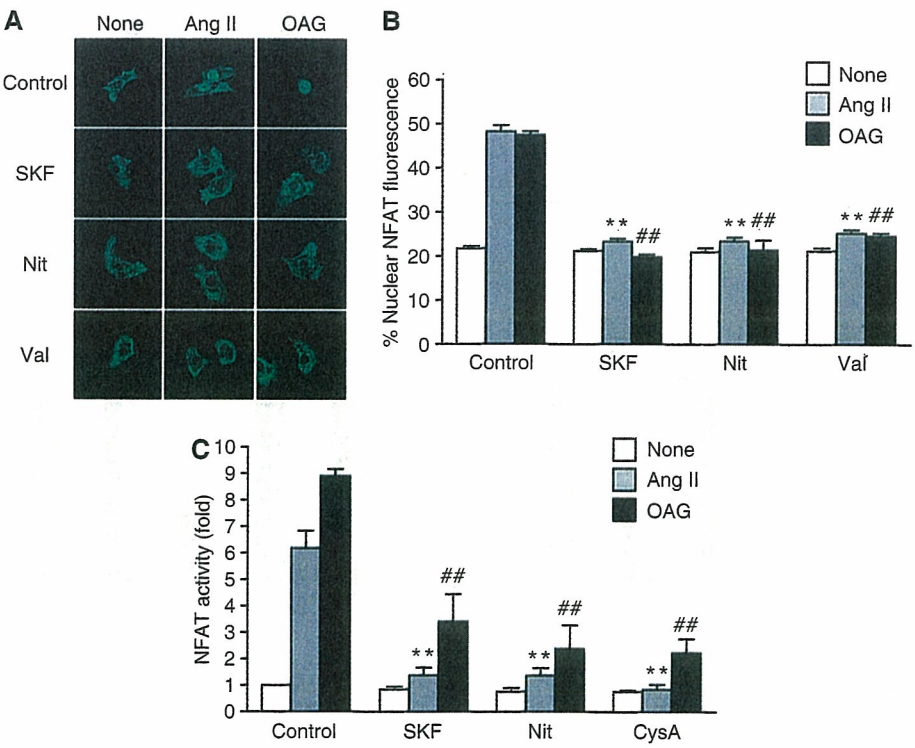

Figure 3 Requirement of RACC and L-type Ca^{2+} channel in DAG-mediated NFAT translocation. (**A**) Effects of SK&F96365 (SKF), nitrendipine (Nit) and valinomycin (Val) on Ang II- or OAG-induced NFAT translocation. (**B**) Quantification of the nuclear predominant fluorescence of GFP-NFAT4 without (None) or with Ang II or OAG stimulation. (**C**) Effects of SKF, Nit, and cyclosporine A (CysA) on Ang II- or OAG-induced increase in NFAT-luciferase activity. Cells were treated with SKF (10 μM), Nit (1 μM), Val (1 μM), or CysA (1 μM) for 30 min before the addition of Ang II (100 nM) or OAG (25 μM). $^{**}P<0.01$ versus Ang II stimulation of control cells. ##; $P<0.01$ versus OAG stimulation of control cells.

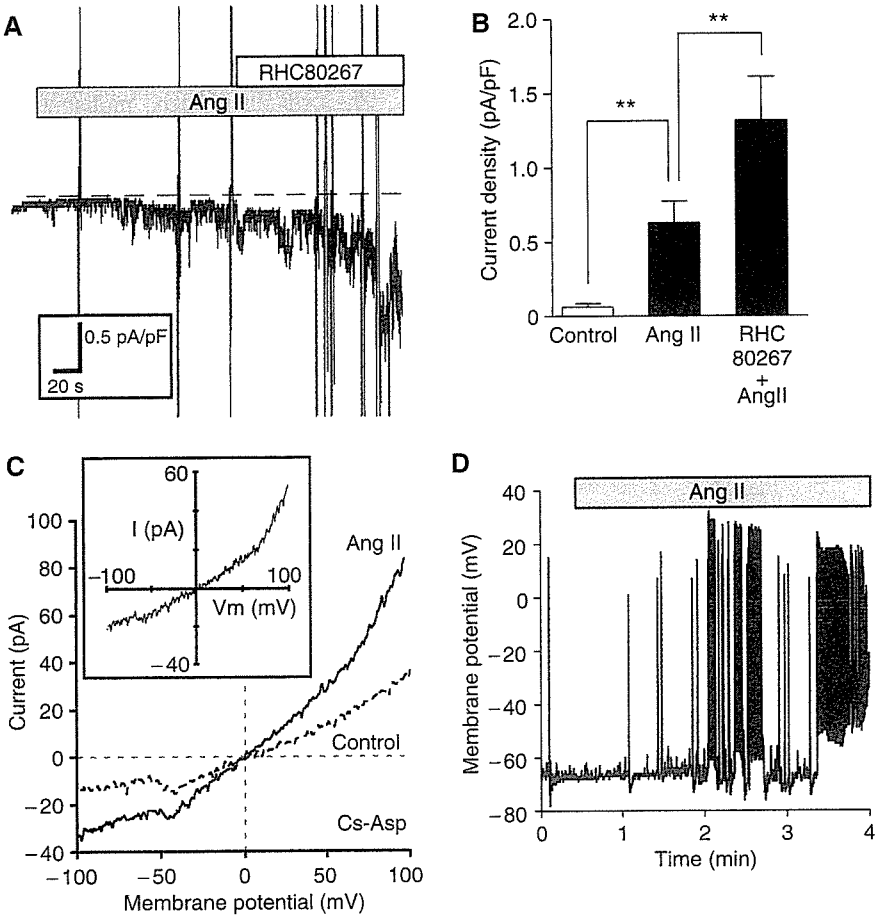

Figure 4 Activation of DAG-sensitive currents from single cardiomyocytes by Ang II stimulation. (**A**) Representative traces of ionic currents recorded from Ang II-treated cardiomyocytes at a holding potential of −80 mV under conventional whole-cell patch-clamp with K^+-internal solution. The nonselective cation currents are activated by Ang II (1 μM), and potentiated by RHC80267 (30 μM). The dotted line represents the zero current level. (**B**) Current density of inward current (at −80 mV) averaged for the period of 60–65 s after Ang II stimulation or RHC80267 treatment ($n>8$). $^{**}P<0.01$. (**C**) *I–V* relationship of ionic currents from unstimulated (Control) and Ang II-stimulated myocytes with Cs^+-internal solution containing myo-IP_3 (10 μM). TTX (3 μM) and nitrendipine (1 μM) are included in the K^+-free external solution. (Inset) *I–V* relationship of TRPC-like currents induced by Ang II (differences between Ang II and Control). (**D**) Representative traces of time-dependent changes in the membrane potential and the frequency of action potential by Ang II stimulation in the current-clamp mode.

K^+-free external solution to block voltage-dependent K^+, Na^+, and L-type Ca^{2+} channels, respectively (see inset in Figure 4C). Administration of OAG (25 μM) also activated inward currents showing indistinguishable properties from those activated by Ang II, whereas application of myo-IP_3 (10 μM) in the internal solution was unable to activate any discernible currents by itself (data not shown). These results collectively suggest that Ang II activates DAG-sensitive nonselective cation currents in cardiomyocytes via an IP_3-independent pathway, which bears considerable resemblance to heterologously expressed TRPC channels.

In the next step, we examined Ang II-induced changes in membrane potential by using the current-clamp technique, since the treatment with valinomycin, a K^+ ionophore, which causes inactivation of voltage-dependent channels via stabilization of membrane potential (Linares-Hernandez *et al*, 1998), completely suppressed the Ang II-induced translocation of GFP-NFAT4 (Figure 3A and B), and in general, the activation of RACC causes membrane depolarization (Large, 2002). As expected, membrane potential recording from single myocytes with current-clamp mode clearly demonstrated that Ang II increased the frequency of action potentials, which eventually led to continuous burstic firing superimposed on concomitant sustained depolarization (22.2 ± 5.6 mV, $n=5$) (Figure 4D). It is noteworthy that the time course of these effects is very similar to that observed for the enhanced frequency of Ca^{2+} oscillations induced by Ang II (see above).

Properties of DAG induced membrane depolarization in rat cardiac myocytes

Current-clamp recordings were technically little feasible to monitor the membrane potential for a long period of time, because of rhythmical contractions of myocytes evoked by Ang II. To circumvent this problem, we adopted a voltage-sensitive fluorescent probe $DiBAC_4(3)$. After $DiBAC_4(3)$ enters the cells, it binds to cellular proteins and membrane lipids. Then, $DiBAC_4(3)$ enhances fluorescence. Because of its slow dissociating nature, $DiBAC_4(3)$ can only detect slow cumulative changes in resting potential rather than rapid changes in membrane potential generated by action potential. Ang II stimulation gradually increased the fluorescence intensity of $DiBAC_4(3)$ (Figure 5A and B), indicating the shift of membrane potential to positive (BACzkó *et al*, 2004). The

averaged changes in membrane potential induced by Ang II were estimated to be ~15 mV. Treatment with RHC80267 enhanced the Ang II-induced increases in the fluorescence intensity of $DiBAC_4(3)$ (Figure 5C). These results indicate that DAG generated by Ang II stimulation shifts the membrane potential of cardiac myocytes more positively. DAG also activates other signaling molecules including protein kinase C (PKC). PKC is known to potentiate the extent of L-type Ca^{2+} channel activation, and both OAG and phorbor 12-myristrate 13-acetate (PMA) have been reported to increase the channel open probability in rat cardiomyocytes (Guinamard *et al*, 2004). However, treatment with PMA did not increase the fluorescence intensity of $DiBAC_4(3)$ (Figure 5A and B) and OAG-induced translocation and activation of NFAT were not affected by bisindolylmaleimide, a selective PKC inhibitor (Supplementary Figure S2). It is possible that

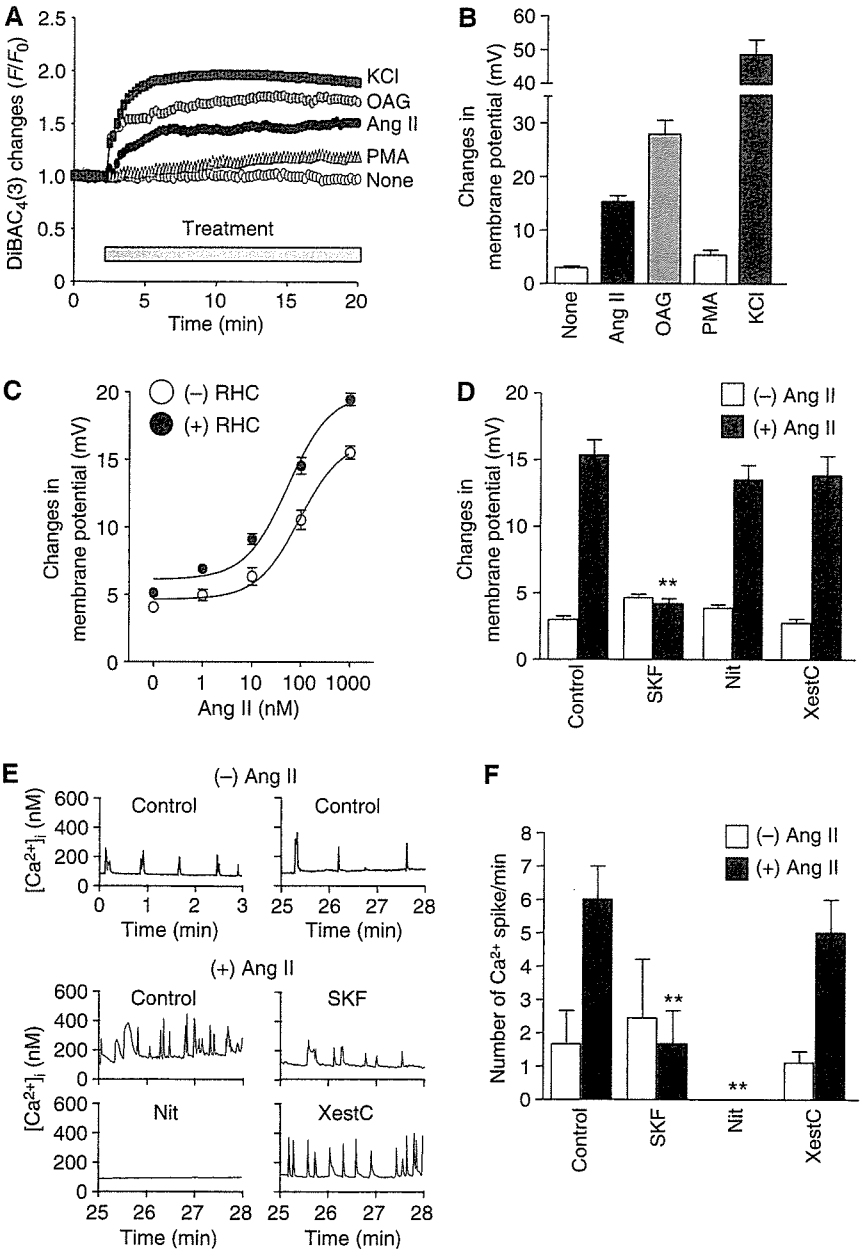

Figure 5 Changes in membrane potential through RACC activation by DAG. (**A**) Representative time courses of changes in Ang II-, OAG-, or PMA-induced F/F_0 of $DiBAC_4(3)$ fluorescence from time course experiments. Cells were stimulated with Ang II (1 μM), OAG (25 μM), PMA (1 μM), or KCl (10 mM). F_0 means the initial value of fluorescence. (**B**) Maximal changes in resting membrane potential calculated from the changes in $DiBAC_4(3)$ fluorescence intensity during 15 min drug treatment. For the *in vivo* calibration of the membrane potentials, the KCl-induced maximal changes in fluorescence were fitted to the theoretical potentials obtained from Nernst equation, and then the changes in membrane potential by Ang II stimulation was calculated based on the fitting fomula. (**C**) Effects of RHC80267 on the concentration-dependent changes in resting membrane potentials induced by Ang II stimulation. (**D**) Involvement of RACC in Ang II-induced increases in the resting membrane potential. Cells were treated with SK&F96365 (SKF, 10 μM), nitredipine (Nit, 1 μM), or xestospongin C (XestC, 20 μM) for 30 min before the addition of Ang II. $^{**}P<0.01$ versus Ang II stimulation of control cells. (**E**) Effects of SK&F96365 (SKF), nitrendipine (Nit), and xestospongin C (XestC) on Ang II-induced Ca^{2+} responses. The digital images were obtained every 1 s during 0–3 min under basal conditions and during 25–28 min after Ang II stimulation. (**F**) Number of Ca^{2+} spikes was normalized to per minute. $^{**}P<0.01$ versus Ang II stimulation of control cells.

the metabolites of DAG work as mediators for NFAT translocation. However, treatment with arachidonic acid (AA) or phospholipase A_2 (PLA_2) inhibitors did not affect Ang II-induced NFAT translocation (Supplementary Figure S2). These results suggest that PKCs and DAG metabolites do not participate in Ang II-induced depolarization and NFAT translocation. The Ang II-induced increases in the fluorescence intensity of $DiBAC_4(3)$ were completely suppressed by SK&F96365, but not by nitrendipine and xestospongin C (Figure 5D).

We next examined whether periodic increase in $[Ca^{2+}]_i$ is regulated by RACC. The myocytes showed spontaneous Ca^{2+} oscillations in the presence of extracellular Ca^{2+} (top panel in Figure 5E). The frequency of Ca^{2+} oscillations was increased by Ang II stimulation and this was suppressed by SK&F96365 and nitrendipine, but not by xestspongin C (middle and bottom panels in Figure 5E and F). These results support the idea that DAG generated by Ang II-induced PLC activation causes membrane depolarization through RACC activation and thereby secondarily activates L-type Ca^{2+} channel, leading to increased frequency of Ca^{2+} oscillations.

Requirement of TRPC3 and TRPC6 in Ang II-induced membrane depolarization

TRPC proteins are thought to be molecular candidates for RACC (Clapham, 2003). We found the expression of at least five TRP canonical (TRPC) mRNAs (TRPC1, TRPC3, TRPC4, TRPC5, TRPC6, and TRPC7) in rat neonatal cardiomyocytes by RT–PCR analysis (data not shown). Recent reports have demonstrated that three TRPC channels (TRPC3, TRPC6, and TRPC7) are activated directly by DAG (Hofmann *et al*, 1999; Clapham, 2003). Thus, we next examined which DAG-sensitive TRPC protein is involved in Ang II-induced NFAT activation. We overexpressed TRPC3, TRPC6, or TRPC7, and examined the Ang II-induced changes in membrane potential with $DiBAC_4(3)$ (Figure 6A and B). Among three TRPC proteins, Ang II-induced increases in the fluorescence intensity of $DiBAC_4(3)$ were significantly enhanced by the expression of TRPC3 and TRPC6 but not by TRPC7 (Figure 6B), although the latter enhanced OAG-induced $[Ca^{2+}]_i$ increases to the same extent as the former two did (Supplementary Figure S3). These results indicate that TRPC3 and TRPC6, but not TRPC7, likely regulate the Ang II-induced membrane depolarization. This conclusion was further corroborated by siRNA-mediated knockdown of TRPC3 (siRNA 1397, 1992, and 2043) and TRPC6 (siRNA 1609 and 1786) in the cardiomyocytes; this procedure decreased the expression level of endogenous TRPC3 and TRPC6 proteins without affecting other TRPC proteins (Figure 6C–F), and simultaneously caused significant suppression of Ang II-induced increases in the fluorescence intensity of $DiBAC_4(3)$ (Figure 6G). Taken together, the above results strongly suggest that DAG-mediated activation of TRPC3 and TRPC6 channels contributes to the enhanced Ca^{2+} oscillation by Ang II via their membrane depolarizing actions.

In addition, siRNA silencing of TRPC3 and TRPC6 also significantly suppressed Ca^{2+} entry-mediated $[Ca^{2+}]_i$ elevation induced by the addition of Ca^{2+} into the bath after Ang II stimulation (Supplementary Figure S3). Thus, some role of direct Ca^{2+} entry via TRPC3/TRPC6-associated pathway cannot completely be excluded in the Ang II-enhanced Ca^{2+} oscillation.

Requirement of TRPC3 and TRPC6 in Ang II-induced NFAT translocation and hypertrophic responses

We next examined whether TRPC3 and TRPC6 are involved in Ang II-induced hypertrophic responses. Treatment with siRNAs of TRPC3 and TRPC6 significantly suppressed Ang II-induced NFAT translocation (Figure 7A and B). Furthermore, both TRPC3 and TRPC6 siRNAs suppressed Ang II-induced actin reorganization and protein synthesis (Figure 7C and D). We further examined the involvement of TRPC6 in Ang II-induced cardiomyocyte hypertrophy by using two dominant negative TRPC6 mutants (Hofmann *et al*, 2002; Hisatsune *et al*, 2004). Expression of TRPC6-Δ(N) and TRPC6-3A significantly suppressed Ang II-induced NFAT activation, actin reorganization, and protein synthesis (Supplementary Figure S4). These results suggest that TRPC3 and TRPC6 play a critical role in Ang II-induced hypertrophic responses in rat neonatal cardiomyocytes.

Discussion

This study reveals the role of DAG in Ang II-induced NFAT activation and hypertrophic responses. DAG produced by Ang II-induced PLC activation directly activates TRPC3 and TRPC6, and the resulting cation (Na^+, Ca^{2+}) influx changes membrane potential to positive, leading to activation of voltage-dependent L-type Ca^{2+} channel possibly through the generation of action potential. The increase in Ca^{2+} influx through L-type Ca^{2+} channel can activate calcineurin/NFAT pathway and hypertrophic responses in rat neonatal cardiomyocytes (Figure 8).

The physiological role of TRPC was first identified in the vascular smooth muscle cells (Inoue *et al*, 2001). In the vascular system, activation of TRPC6 contributes to membrane depolarization and regulates myogenic tone of resistance arteries (Large, 2002; Welsh *et al*, 2002). In the present study, we demonstrated that TRPC3 and TRPC6 activated by DAG contributes to the shift of membrane potential and subsequent Ca^{2+} signal generation through voltage-dependent Ca^{2+} channel in cardiac myocytes. The role of DAG-induced TRPC3 and TRPC6 activation in membrane depolarization has been reported in vascular smooth muscle cells (Reading *et al*, 2005; Soboloff *et al*, 2005). The novel finding of the present study is to characterize the pathophysiological significance of TRPC3 and TRPC6 in Ang II-induced hypertrophic responses of the heart.

We cannot determine the subtype(s) of TRPC proteins activated by Ang II from the *I–V* relationship of native RACC, as inward current activated by Ang II was too small (Figure 4). Previous report has shown that fulfenamate inhibits TRPC3 but enhances TRPC6 channel activity (Inoue *et al*, 2001). The Ang II-induced inward current was slightly inhibited by flufenamate (data not shown). However, the similar behavior of currents to the present study was reported in TRPC3/C6-co-expressing HEK293 cells (Maruyama *et al*, 2006). TRPC3-like currents were observed by coexpression of TRPC3 and TRPC6. As Ang II-induced responses were inhibited both by siRNAs of TRPC3 and TRPC6 (Figures 6 and 7), we speculate that TRPC3 and TRPC6 form heterotetramers to regulate DAG-sensitive native cationic currents in cardiac myocytes.

In our hands, the expression of TRPC7 did not enhance Ang II-induced membrane depolarization (Figure 6B). This

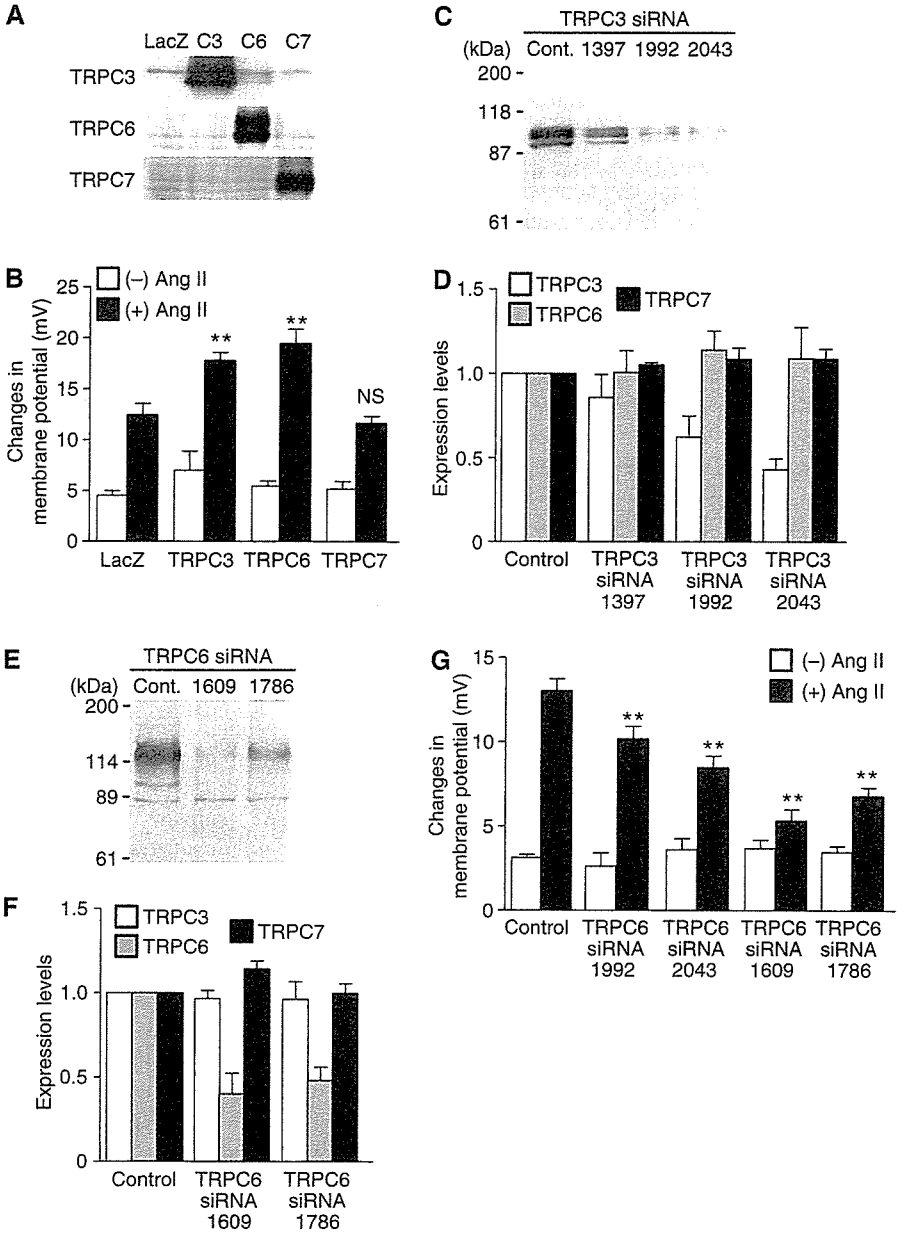

Figure 6 Requirement of TRPC3 and TRPC6 in Ang II-induced increases in membrane potential. (**A**) Western blots of the respective TRPC proteins. To identify the sizes of TRPC3 (C3), TRPC6 (C6), and TRPC7 (C7), each TRPC was overexpressed with recombinant adenoviruses. (**B**) Potentiating effects of TRPC3 and TRPC6 on changes in membrane potential by Ang II stimulation in LacZ-, TRPC3-, TRPC6-, and TRPC7-expressing cells. $^{**}P<0.01$ versus Ang II stimulation of LacZ-expressing cells. NS means no significance from LacZ-expressing cells. (C–F) Effects of TRPC3 siRNAs (**C, D**) and TRPC6 siRNAs (**E, F**) on the expression of the respective TRPC proteins. (C, E) Representative Western blots with anti-TRPC3 (C) and anti-TRPC6 (E). (D, F) Effects of siRNAs of TRPC3 and TRPC6 on the average expression of native TRPC3, TRPC6, and TRPC7 proteins. (**G**) Effects of siRNAs of TRPC3 and TRPC6 on the maximal changes in $DiBAC_4(3)$ fluorescence intensity by Ang II (100 nM). Data are shown as the changes in membrane potentials (mV) calculated by *in vivo* calibration. $^{**}P<0.01$ versus Ang II stimulation of control siRNA-treated cells (Control).

may be explained by differential spatial organization and dynamics in the receptor-transduction systems (Delmas *et al*, 2002). As OAG-induced increases in $[Ca^{2+}]_i$, but Ang II-induced shift of membrane potential, was not enhanced in TRPC7-expressing cells (Supplementary Figure S3, Figure 6B), Ang II signaling microdomain may contain TRPC6 and TRPC3, but not TRPC7. This idea is supported by the reports that stimulation of AT1R activates TRPC6 (Large, 2002; Winn *et al*, 2005).

Previous report suggested that capacitative Ca^{2+} entry contributes to the nuclear translocation of NFAT and hypertrophy in cardiomyocytes (Hunton *et al*, 2002). In contrast with the present study, they showed that IP_3-mediated store depletion triggers the activation of SOC and activates hypertrophic responses. Although we cannot explain the discrepancy between their report and the present study, we clearly demonstrated that xestospongin C or IP_3-sponge did not affect Ang II-induced changes in fluorescence intensity of $DiBAC_4(3)$, NFAT activation, and hypertrophic responses (Figures 1 and 5D). We also confirmed that the application of high concentration of IP_3 did not activate whole-cell currents (data not shown). In addition, treatment with

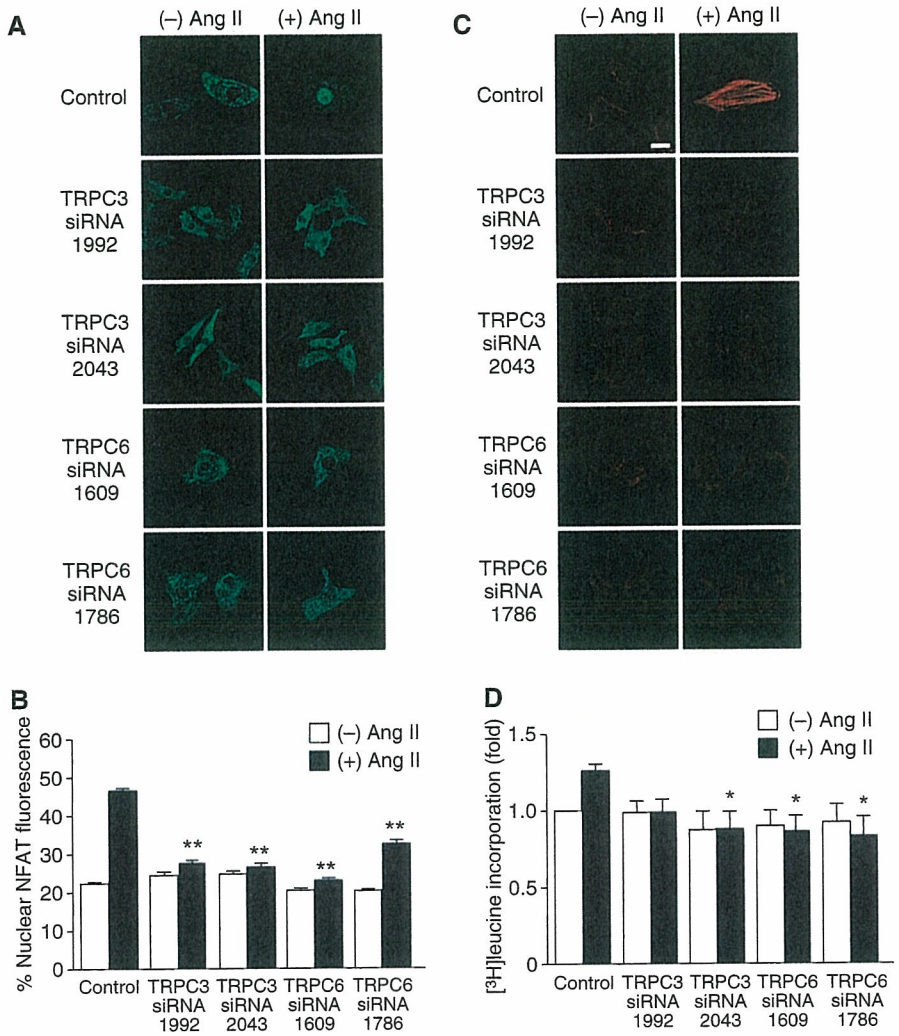

Figure 7 Requirement of TRPC3 and TRPC6 in Ang II-induced hypertrophic responses. Effects of siRNAs of TRPC3 and TRPC6 on Ang II-induced NFAT translocation (**A, B**), actin reorganization (**C**), and protein synthesis (**D**). Scale bar = 20 μm. $*P<0.05$, $**P<0.01$ versus Ang II stimulation of control siRNA-treated cells (Control).

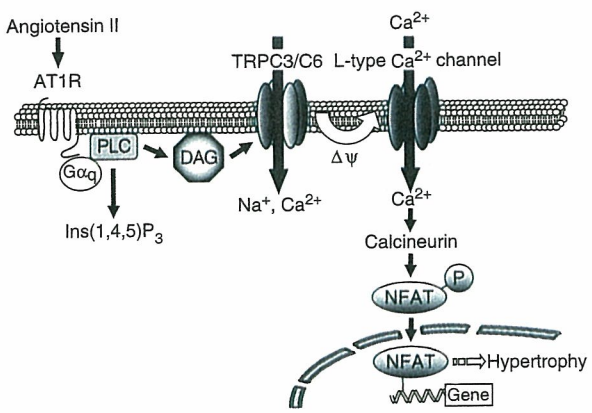

Figure 8 Schema of Ang II-induced NFAT activation in cardiac myocytes. In cardiac myocytes, stimulation of AT1R induces NFAT activation through $G\alpha_q$-PLC signaling pathway. DAG, generated by PLC activation, directly activates TRPC3 and TRPC6 (TRPC3/C6). Activation of TRPC3/C6 causes slow increases in the membrane potential to a positive direction ($\Delta\Psi$) and concomitantly increases the frequency of spontaneous firing due to activation of L-type Ca^{2+} channel. The Ca^{2+} influx though L-type Ca^{2+} channel activates calcineurin-NFAT pathway, which leads to hypertrophic responses in cardiomyocytes.

caged-IP_3 did not affect the localization of GFP-NFAT4 upon UV irradiation, although caged-IP_3 induced a marked increases in $[Ca^{2+}]_i$ (Supplementary Figure 5). We observed that the treatments with thapsigargin and ionomycin induce NFAT activation through store-operated Ca^{2+} influx. However, Ang II-stimulated increase in $[Ca^{2+}]_i$ through IP_3-mediated Ca^{2+} release is 25–30% of those induced by thapsigargin and ionomycin treatment. This IP_3-mediated increase may not be enough for the activation of SOC. These results suggest that IP_3-mediated Ca^{2+} signaling, including SOC, is not responsible for Ang II-induced NFAT activation.

Whole-cell current experiments revealed that the membrane currents were activated more than 1 min after Ang II stimulation (Figure 4A). However, the maximal shift of membrane potential was achieved about 2 min after Ang II stimulation (Figure 5A). The distinct delay may be explained by DAG metabolism, as RHC80267 enhanced Ang II-induced inward current (Figure 4B). The steady-state DAG lipase activity may regulate the time to elevate DAG concentration required for the activation of whole-cell currents and subsequent changes in membrane potential.

Growing evidence has indicated the involvement of L-type Ca^{2+} channels in the induction of cardiac hypertrophy (Lubic *et al*, 1994, 1995; Whitehurst *et al*, 1999; Liao *et al*, 2005). The role of L-type Ca^{2+} channels in excitation-transcription coupling is well established in the nervous system (Dolmetsch *et al*, 2001, 2003). Calmodulin is reported to be critical for conveying the Ca^{2+} signal to the nucleus (Dolmetsch *et al*, 2001). As calmodulin also regulates calcineurin activity, calmodulin may convey the signal to the nucleus in the cardiovascular system in a similar manner to the nervous system.

While this study is in review process, Bush *et al* (2006) reported that TRPC channels are involved in hypertrophy through pathological calcineurin/NFAT signaling. They showed that TRPC3 expression is upregulated in mice with pathological hypertrophy. We demonstrated that TRPC3 and TRPC6 mediate hypertrophic responses of neonatal myocytes by Ang II stimulation. Thus, the upregulated TRPC channels *in vivo* may enhance receptor-stimulated hypertrophy through the mechanism that we have demonstrated in this study.

In summary, we demonstrated for the first time that PLC-generated DAG has a pathophysiological role in activation of TRPC3 and TRPC6, and TRPC3/6 mediates NFAT-mediated hypertrophic responses through L-type Ca^{2+} channel.

Materials and methods

Materials, plasmid construction, and cell cultures

AT1R blocker CV11974 was provided from Takeda Chemical Industries Ltd (Osaka, Japan). PTX, SK&F96365, caged-IP_3, and $cPLA_2$ inhibitor were purchased from Calbiochem. Valinomycin, cyclosporine A, U73122, U73343, AA, $PACOCF_3$, myo-IP_3, TTX, and PD123319 were from Sigma. Fura2/AM was from Dojindo. Collagenase, Liberase (enzyme 3), and Fugene 6 were from Roche. Alexa Fluor 594-phalloidin and $DiBAC_4(3)$ were from Molecular Probe. Nitrendipine was from Wako. The cDNA coding DGKβ (KIAA0718) was obtained from Kazusa DNA Research Institute. The cDNAs coding mouse TRPC3, TRPC6, and TRPC7, and anti-TRPC7 antibody were prepared as described (Inoue *et al*, 2001; Nishida *et al*, 2003). Anti-TRPC6 and anti-TRPC3 antibodies were from Alomone. Mouse TRPC6-3A and TRPC6-Δ(N) were constructed according to the previous reports (Hofmann *et al*, 2002; Hisatsune *et al*, 2004). The cDNA coding IP_3-sponge was cloned from mouse brain (Uchiyama *et al*, 2002), and GFP-IP_3-sponge was constructed in pEGFP-C1 vector (Clontech). Isolation of rat neonatal cardiomyocytes was described (Nishida *et al*, 2000).

Production of adenoviruses, infection, and transfection

Recombinant adenoviruses of GFP-NFAT4, HA-tagged DGKβ, GFP-DGKβ, wild-type TRPC6, TRPC6-3A, TRPC6-Δ(N), and GFP-fused IP_3-sponge (GFP-IP_3-sponge) were produced by the method of He *et al* (1998) with a slight modification. Other adenoviruses were prepared as described previously (Nishida *et al*, 2000, 2005; Arai *et al*, 2003). Cells were infected with adenovirus(es) at 100 MOI for 48 h. Small interference RNAs (250 nM) were transfected with lipofectamine 2000 for 72 h.

Measurement of NFAT activity

Measurement of NFAT activity was performed as described previously (Fujii *et al*, 2005). At 2 h after adenoviral infection in serum-free medium, cardiomyocytes (1×10^6 cells) plated on 24-well dishes were transiently cotransfected with 0.45 μg pNFAT-Luc and 0.05 μg pRL-SV40 control plasmid, using Fugene 6. For measuring the translocation of GFP-NFAT4, cells (1×10^6) plated on glass-bottom 35 mm dishes were infected for 48 h with adenovirus coding GFP-NFAT4 at 100 MOI. After Ang II stimulation (100 nM) for 30 min, the localization of GFP-NFAT4 was determined with a Laser Scanning Confocal Imaging System (Carl Zeiss LSM510) as described (Fujii *et al*, 2005).

Measurement of $[Ca^{2+}]_i$ and membrane potential

The intracellular Ca^{2+} concentration ($[Ca^{2+}]_i$) of cardiomyocytes was determined as described (Arai *et al*, 2003; Nishida *et al*, 2005). Briefly, cells (1×10^6) were plated on gelatin-coated glass-bottom 35 mm dishes and were loaded with 2.5 μM fura-2/AM at 37°C for 30 min. For measurement of cell membrane potential, cells were loaded with 1.5 μM $DiBAC_4(3)$ at 37°C for 30 min. The fluorescence intensity of $DiBAC_4(3)$ was measured at an excitation wavelength of 488 nm with a video image analysis system (Aquacosmos, Hamamatsu Photonics). The peak changes ($\Delta F/F_0$) of $DiBAC_4(3)$ fluorescence intensity were defined as values obtained by subtracting the basal fluorescence intensity (F_0) from the maximal intensity during 19 min Ang II treatment.

Measurement of the expression of TRPC proteins

Cardiomyocytes (3×10^6 cells) plated on six-well dishes were directly harvested with 2 × SDS sample buffer. The protein samples were fractionated by 8% SDS–PAGE gel and then transferred onto PVDF membrane. The expression of endogenous TRPC proteins was assessed by Western blotting using anti-TRPC antibodies. To examine the involvement of TRPC3 and C6, knockdown experiments using siRNAs were performed (sequences of siRNAs used in this study were presented in Supplementary Table 1). We used Stealth (Invitrogen) siRNA sequence to eliminate nonspecific responses by siRNA. Transfection was performed by lipofectamine 2000.

Measurement of hypertrophic responses of cardiomyocytes

Measurement of cardiomyocyte hypertrophy was performed as described (Maruyama *et al*, 2002). Briefly, 24 h after infection, cardiomyocytes were stimulated with Ang II (100 nM) for 48 h. The cells were washed, fixed, and then stained with Alexa Fluor 594-phalloidin to visualize actin filaments. Protein synthesis was measured by [^{3}H]leucine incorporation. After cells were stimulated with Ang II (100 nM) for 18 h, [^{3}H]leucine (1 μCi/ml) was add to the culture medium and further incubated for 6 h. The incorporated [^{3}H]leucine was measured using liquid-scintillation counter.

Electrophysiology

Single neonatal rat cardiac myocytes plated on thin coverslips for 1–2 days (3 × 10 mm; Matsunami, Japan) were used for patch-clamp experiments. The details of patch-clamp experiments are described elsewhere (Shi *et al*, 2004). Internal solution used for the whole-cell variant of patch clamp; K^+-internal solution (mM): 140 K^+, 4 Na^+, 2 Mg^{2+}, 144 Cl^-, 2 EGTA, 2 ATP, 10 HEPES or Cs^+-internal solution (mM): 140 Cs^+, 2 Mg^{2+}, 20 Cl^-, 2 SO_4^{2-}, 120 aspartate, 2 ATP, 5 EGTA (2 Ca^{2+} added), 10 HEPES, and 10 μM myo-IP_3. For current-clamp recordings, normal external solution and K^+-internal solution of the same composition as used for whole-cell voltage-clamp experiments were used. All experiments were performed at 25–28°C with the aid of a temperature control unit (Warner Instruments) to facilitate the response to Ang II.

Statistical analysis

The results are shown as means±s.e.m. All experiments were repeated at least three times. Mean values were compared with control by Student's *t*-test (for two groups) or one-way ANOVA followed by Dunnett's *t*-test (for three or more groups).

Supplementary data

Supplementary data are available at *The EMBO Journal* Online (http://www.embojournal.org).

Acknowledgements

We thank Y Ito (Department of Pharmacology, Graduate School of Medical Sciences, Kyushu University) for using Aquacosmos imaging system during early stage of this study. We also thank SM Lanier and M Sato (Louisiana State University Health Science Center) for experimental suggestion, and T Murakami for DNA construction. This work was supported by grants from the Ministry of Education, Culture, Sports, Science and Technology of Japan (to M Nishida and H Kurose), from Ministry of Health, Labour and Welfare of Japan, and the National Institute of Biomedical

Innovation (MF-16, to YS), and by grants from The Naito Foundation, The Kanae Foundation, The Suzuken Memorial Foundation, The Uehara Memorial Foundation, Kao Foundation for Arts and Sciences, Takeda Science Foundation and Japan Heart Foundation Research Grant (to MN), and Astellas Foundation for Research on Metabolic Disorders (H Kurose).

References

Arai K, Maruyama Y, Nishida M, Tanabe S, Takagahara S, Kozasa T, Mori Y, Nagao T, Kurose H (2003) Endothelin-1-induced MAPK activation and cardiomyocyte hypertrophy are mediated by $G\alpha_{12}$ and $G\alpha_{13}$ as well as $G\alpha_q$ and $G\beta\gamma$ subunits. *Mol Pharmacol* **63:** 478–488

BACzkó I, Giles WR, Light PE (2004) Pharmacological activation of plasma-membrane K_{ATP} channels reduces reoxygenation-induced Ca^{2+} overload in cardiac myocytes via modulation of the diastolic membrane potential. *Br J Pharmacol* **141:** 1059–1067

Bush EW, Hood DB, Papst PJ, Chapo JA, Minobe W, Bristow MR, Olson EN, McKinsey TA (2006) TRPC channels promote cardiomyocyte hypertrophy through activation of calcineurin signaling. *J Biol Chem*, (in press) (doi: 10.1074/jbc.M605536200)

Clapham DE (2003) TRP channels as cellular sensors. *Nature* **426:** 517–524

Crabtree GR, Olson EN (2002) NFAT signaling: choreographing the social lives of cells. *Cell* **109:** S67–S79

Delmas P, Wanaverbecq N, Abogadie FC, Mistry M, Brown DA (2002) Signaling microdomains define the specificity of receptor-mediated InsP3 pathways in neurons. *Neuron* **34:** 209–220

Dolmetsch R (2003) Excitation-transcription coupling: signaling by ion channels to the nucleus. *Science's stke*, www.stke.org/cgi/content/full/sigtrans;2003/166/pe4

Dolmetsch RE, Lewis RS, Goodnow CC, Healy JI (1997) Differential activation of transcription factors induced by Ca^{2+} response amplitude and duration. *Nature* **386:** 855–858

Dolmetsch RE, Pajvani U, Fife K, Spotts JM, Greenberg ME (2001) Signaling to the nucleus by an L-type calcium channel-calmodulin complex through the MAP kinase pathway. *Science* **294:** 333–339

Dostal DE, Rothblum KN, Chernin MI, Cooper GR, Baker KM (1992) Intracardiac detection of angiotensinogen and renin: a localized rennin–angiotensin system in neonatal rat heart. *Am J Physiol* **263:** C838–C850

Fujii T, Onohara N, Maruyama Y, Tanabe S, Kobayashi H, Fukutomi M, Nagamatsu Y, Nishihara N, Inoue R, Sumimoto H, Shibasaki F, Nagao T, Nishida M, Kurose H (2005) $G\alpha_{12/13}$-mediated production of reactive oxygen species is critical for angiotensin receptor-induced NFAT activation in cardiac fibroblasts. *J Biol Chem* **280:** 23041–23047

Guinamard R, Chatelier A, Lenfant J, Bois P (2004) Activation of the Ca^{2+}-activated nonselective cation channel by diacylglycerol analogues in rat cardiomyocytes. *J Cardiovas Electrophysiol* **15:** 342–348

He TC, Zhou S, da Costa LT, Yu J, KInzler KW, Vogelstein B (1998) A simplified system for generating recombinant adenoviruses. *Proc Natl Acad Sci USA* **95:** 2509–2514

He Y, Yao G, Savoia C, Touyz RM (2005) Transient receptor potential melastatin 7 ion channels regulate magnesium homeostasis in vascular smooth muscle cells. Role of angiotensin II. *Circ Res* **96:** 207–215

Hisatsune C, Kuroda Y, Nakamura K, Inoue T, Nakamura T, Michikawa T, Mizutani A, Mikoshiba K (2004) Regulation of TRPC6 channel activity by tyrosine phosphorylation. *J Biol Chem* **279:** 18887–18894

Hofmann T, Obukhov AG, Schaefer M, Harteneck C, Gudermann T, Schultz G (1999) Direct activation of human TRPC6 and TRPC3 channels by diacylglycerol. *Nature* **397:** 259–263

Hofmann T, Schaefer M, Schultz G, Gudermann T (2002) Subunit composition of mammalian transient receptor potential channels in living cells. *Proc Natl Acad Sci USA* **99:** 7461–7466

Hunton DL, Lucchesi PA, Pang Y, Cheng X, Dell'Italia LJ, Marchase RB (2002) Capacitative calcium entry contributes to nuclear factor of activated T cells nuclear translocation and hypertrophy in cardiomyocytes. *J Biol Chem* **277:** 14266–14273

Inoue R, Okada T, Onoue H, Hara Y, Shimizu S, Naitoh S, Ito Y, Mori Y (2001) The transient receptor potential protein homologue TRP6 is the essential component of vascular α_1-adrenoceptor-activated Ca^{2+}-permeable cation channel. *Circ Res* **88:** 325–332

Large WA (2002) Receptor-operated Ca^{2+}-permeable nonselective cation channels in vascular smooth muscle: a physiologic perspective. *J Cardiovas Electrophysiol* **13:** 493–501

Liao Y, Asakura M, Takashima S, Kato H, Asano Y, Shintani Y, Minamino T, Tomoike H, Hori M, Kitakaze M (2005) Amlodipine ameliorates myocardial hypertrophy by inhibiting EGFR phosphorylation. *Biochem Biophys Res Commun* **327:** 1083–1087

Linares-Hernandez L, Guzman-Grenfell AM, Hicks-Gomez JJ, Gonzalez-Martinez MT (1998) Voltage dependent calcium influx in human sperm assessed by spontaneous detection of intracellular calcium and membrane potential. *Biochem Biophys Acta* **1372:** 1–12

Lubic SP, Giacomini KM, Giacomini JC (1994) Increased 1,4-dihydropyridine binding sites in serum-stimulated cardiomyocytes hypertrophy. *J Pharmacol Exp Ther* **270:** 697–701

Lubic SP, Giacomini KM, Giacomini JC (1995) The effects of modulation of calcium influx through the voltage-sensitive calcium channel on cardiomyocyte hypertrophy. *J Mol Cell Cardiol* **27:** 917–925

Maruyama Y, Nakanishi Y, Walsh EJ, Wilson DP, Welsh DG, Cole WC (2006) Heteromultimeric TRPC6-TRPC7 channels contribute to arginine vasopressin-induced cation current of A7r5 vascular smooth muscle cells. *Circ Res* **98:** 1520–1527

Maruyama Y, Nishida M, Sugimoto Y, Tanabe S, Turner JH, Kozasa T, Wada T, Nagao T, Kurose H (2002) $G\alpha_{12/13}$ mediate α_1-adrenergic receptor-induced cardiac hypertrophy. *Circ Res* **91:** 961–969

Molkentin JD, Dorn II GW (2001) Cytoplasmic signaling pathways that regulate cardiac hypertrophy. *Annu Rev Physiol* **63:** 391–426

Molkentin JD, Lu JR, Antos CL, Markham B, Richardson J, Robbins J, Grant SR, Olson EN (1998) A calcineurin-dependent transcriptional pathway for cardiac hypertrophy. *Cell* **93:** 215–228

Moschella MC, Marks AR (1993) Inositol 1,4,5-trisphosphate receptor expression in cardiac myocytes. *J Clin Invest* **120:** 1137–1146

Nishida M, Maruyama Y, Tanaka R, Kontani K, Nagao T, Kurose H (2000) $G\alpha_i$ and $G\alpha_o$ are target proteins of reactive oxygen species. *Nature* **408:** 492–495

Nishida M, Sugimoto K, Hara Y, Mori E, Morii T, Kurosaki T, Mori Y (2003) Amplification of receptor signalling by Ca^{2+} entry-mediated translocation and activation of PLCγ2 in B lymphocytes. *EMBO J* **22:** 4677–4688

Nishida M, Tanabe S, Maruyama Y, Mangmool S, Urayama K, Nagamatsu Y, Takagahara S, Turner JH, Kozasa T, Kobayashi H, Sato Y, Kawanishi T, Inoue R, Nagao T, Kurose H (2005) $G\alpha_{12/13}$- and reactive oxygen species-dependent activation of c-Jun NH_2-terminal kinase and p38 MAPK by angiotensin receptor stimulation in rat neonatal cardiomyocytes. *J Biol Chem* **280:** 18434–18441

Reading SA, Early S, Waldron BJ, Welsh DG, Brayden JE (2005) TRPC3 mediates pyrimidine receptor-induced depolarization of cerebral arteries. *Am J Physiol* **288:** H2055–H2061

Sadoshima J, Xu Y, Slayter HS, Izumo S (1993) Autocrine release of angiotensin II mediates stretch-induced hypertrophy of cardiac myocytes *in vitro*. *Cell* **75:** 977–984

Seth M, Sumbilla C, Mullen SP, Lewis D, Klein G, Hussain A, Soboloff J, Gill DL, Inesi G (2004) Sarco(endo)plasmic reticulum Ca^{2+} ATPase (SERCA) gene silencing and remodeling of the Ca^{2+} signaling mechanism in cardiac myocytes. *Proc Natl Acd Sci USA* **101:** 16683–16688

Shi J, Mori E, Mori Y, Mori M, Li J, Ito Y, Inoue R (2004) Multiple regulation by calcium of murine homologues of transient receptor potential proteins TRPC6 and TRPC7 expressed in HEK293 cells. *J Physiol* **561:** 415–432

Soboloff J, Spassova M, Xu W, He LP, Cuesta N, Gill DL (2005) Role of endogenous TRPC6 channels in Ca^{2+} signal generation in A7r5 smooth muscle cells. *J Biol Chem* **280:** 39786–39794

Taigen T, De Windt LJ, Lim HW, Molkentin JD (2000) Targeted inhibition of calcineurin prevents agonist-induced cardiomyocyte hypertrophy. *Proc Natl Acd Sci USA* **97:** 1196–1201

Timmerman LA, Clipstone NA, Ho SN, Northrop JP, Crabtree GR (1996) Rapid shuttling of NF-AT in discrimination of Ca^{2+} signals and immunosuppression. *Nature* **383:** 837–840

Tomida T, Hirose K, Takizawa A, Shibasaki F, Iino M (2003) NFAT functions as a working memory of Ca^{2+} signals in decoding Ca^{2+} oscillation. *EMBO J* **22:** 3825–3832

Touyz RM, He Y, Montezano ACI, Yao G, Chubanov V, Gudermann T, Callera GE (2006) Differential regulation of transient receptor potential melastatin 6 and 7 cation channels by ANG II in vascular smooth muscle cells from spontaneous hypertensive rats. *Am J Physiol* **290:** R73–R78

Uchiyama T, Yoshikawa F, Hishida A, Furuichi T, Mikoshiba K (2002) A novel recombinant hyperaffinity inositol 1,4,5 -trisphosphate (IP_3) absorbent traps IP_3, resulting in specific inhibition of IP_3-mediated calcium signaling. *J Biol Chem* **277:** 8106–8113

Welsh DG, Morielli AD, Nelson MT, Brayden JE (2002) Transient receptor potential channels regulate myogenic tone of resistance arteries. *Circ Res* **90:** 248–250

Whitehurst Jr RM, Zhang M, Bhattacharjee A, Li M (1999) Dexamethasone-induced hypertrophy in rat neonatal cardiac myocytes involves an elevated L-type Ca^{2+} current. *J Mol Cell Cardiol* **31:** 1551–1558

Wilkins BJ, De Windt LJ, Bueno OF, Braz JC, Glascock BJ, Kimball TF, Molkentin JD (2002) Targeted disruption of NFATc3, but not NFATc4, reveals an intrinsic defect in calcineurin-mediated cardiac hypertrophic growth. *Mol Cell Biol* **22:** 7603–7613

Wilkins BJ, Molkentin JD (2004) Calcium-calcineurin signaling in the regulation of cardiac hypertrophy. *Biochem Biophys Res Commun* **322:** 1178–1191

Winn MP, Conlon PJ, Lynn KL, Farrington MK, Creazzo T, Hawkins AF, Daskalakis N, Kwan SY, Ebersviller S, Burchette JL, Pericak-Vance MA, Howell DN, Vance JM, Rosenberg PB (2005) A mutation of TRPC6 cation channel causes familial focal segmental glomerulosclerosis. *Science* **308:** 1801–1804

Woodcock EA, Matkovich SJ (2005) Ins(1,4,5)P_3 receptors and inositol phosphates in the heart-evolutionary artifacts or active signal transducers? *Pharmacol Therap* **107:** 240–251